Large area smoothing of surfaces by ion bombardment: fundamentals and applications

2009 J. Phys.: Condens. Matter 21 224026

(http://iopscience.iop.org/0953-8984/21/22/224026)

IOP Publishing Journal of Physics: Condensed Matter

J. Phys.: Condens. Matter **21** (2009) 224026 (20pp) doi:10.1088/0953-8984/21/22/224026

TOPICAL REVIEW

Large area smoothing of surfaces by ion bombardment: fundamentals and applications

F Frost, R Fechner, B Ziberi, J Völlner, D Flamm and A Schindler

Leibniz-Institut für Oberflächenmodifizierung e. V. (IOM), Permoserstraße 15, D-04318 Leipzig, Germany

E-mail: frank.frost@iom-leipzig.de

Received 11 February 2009
Published 12 May 2009
Online at stacks.iop.org/JPhysCM/21/224026

Abstract

Ion beam erosion can be used as a process for achieving surface smoothing at microscopic length scales and for the preparation of ultrasmooth surfaces, as an alternative to nanostructuring of various surfaces via self-organization. This requires that in the evolution of the surface topography different relaxation mechanisms dominate over the roughening, and smoothing of initially rough surfaces can occur. This contribution focuses on the basic mechanisms as well as potential applications of surface smoothing using low energy ion beams.

In the first part, the fundamentals for the smoothing of III/V semiconductors, Si and quartz glass surfaces using low energy ion beams (ion energy: $\leqslant$2000 eV) are reviewed using examples. The topography evolution of these surfaces with respect to different process parameters (ion energy, ion incidence angle, erosion time, sample rotation) has been investigated. On the basis of the time evolution of different roughness parameters, the relevant surface relaxation mechanisms responsible for surface smoothing are discussed. In this context, physical constraints as regards the effectiveness of surface smoothing by direct ion bombardment will also be addressed and furthermore ion beam assisted smoothing techniques are introduced.

In the second application-orientated part, recent technological developments related to ion beam assisted smoothing of optically relevant surfaces are summarized. It will be demonstrated that smoothing by direct ion bombardment in combination with the use of sacrificial smoothing layers and the utilization of appropriate broad beam ion sources enables the polishing of various technologically important surfaces down to 0.1 nm root mean square roughness level, showing great promise for large area surface processing. Specific examples are given for ion beam smoothing of different optical surfaces, especially for substrates used for advanced optical applications (e.g., in x-ray optics and components for extreme ultraviolet lithography).

(Some figures in this article are in colour only in the electronic version)

Contents

1. Introduction

Ion beam sputtering or ion beam erosion of surfaces can generate a diversity of surface topographies, as has been reviewed and discussed in this special issue with the focus on nanopatterning via self-organization. Typically, during ion beam sputtering, the surface of the solid is far from equilibrium and a variety of atomistic surface processes and mechanisms become effective. It is the complex interplay of these processes that either tends to roughen (e.g., by curvature dependent sputtering) or smooth (e.g., by surface diffusion or viscous flow of surface atoms) the surface, which, finally, can result in the spontaneous formation of patterns. Extensive experimental and theoretical studies, recently summarized in different reviews [1–6], have shown that a multitude of nanopatterns can occur, depending on ion beam sputtering conditions and on the respective material properties.

As mentioned before, current activities in the investigations of the surface evolution during low energy ion beam erosion are mainly motivated by the intriguing possibilities offered by ion beams as a simple, massively parallel, and therefore cost-efficient, approach for nanostructuring of surfaces via self-organization.

Seen in a historical context, however, many of the earlier studies on surface evolution were driven by the effort to minimize surface roughening by energetic ions. Thus roughness induced by the stepwise or continuous removal of thin surface layers by ion beam sputtering is very critical for surface cleaning processes and many depth profiling analytical techniques like secondary-ion mass spectrometry (SIMS) and Auger electron spectroscopy (AES) [7–15]. In microtechnology and nanotechnology using ion beam and plasma etching fabrication techniques the roughness evolution of the etched surfaces is very crucial for the operation and quality of optical components and electronic devices, which becomes more and more important with shrinking device dimension [16].

Another important field of application of ion beams is the manufacturing of ultraprecise and ultrasmooth surfaces [17–19]. Nowadays, ultrasmooth surfaces are gaining in importance, for example in the fields of conventional optics, magnetic storage technology, semiconductor technology, and the more sophisticated optical elements used for different spectral ranges (extreme ultraviolet (EUV), soft x-rays) or neutron optics. A specific example is the fabrication of ultrasmooth diamond-like carbon surfaces, as a key for ultrahigh storage density hard disks [20].

In the field of optics, probably the most stringent conditions for surface accuracy and smoothness are made on optical components for DUV (deep ultraviolet) and EUV lithography (EUVL) [21, 22]. Today it is expected that for the fabrication of integrated circuits EUVL will have pilot scale applications at the 32 nm technology node and will be used in full production for the 22 nm half-pitch technology node with the capability to extend to the next technology node [21]. For EUVL optical systems, reflective optics have to be used for all parts of the system (illumination optics, mask, projection optics), because all available materials are absorbing in the EUV spectral range and no material is transparent enough for use as refractive optics. Therefore, near normal incident EUV light is reflected by multilayer mirrors (Bragg mirrors) made of molybdenum and silicon (Mo/Si) multilayer with a period designed for a wavelength of 13.5 nm [23–27]. For the mirror substrates used, a surface precision in the subnanometer range root mean square (rms) of deviations from the ideal mathematical design over the entire range of spatial dimensions from the full aperture down to the nanometer scale roughness on all surfaces have to be realized in fabrication [21]. The so-called fine surface figure error includes all spatial wavelengths longer than 1 mm up to full aperture of the mirror. Typically, the related error has to be $\leqslant$0.1 nm rms in order to reduce aberrations and flare. Similar rms values are required for the mid-spatial frequency roughness (MSFR, typically $\leqslant$0.15 nm rms) that covers spatial periods between 1 mm and 1 μm, and for the high spatial frequency roughness (HSFR, typically in the range of 0.1 nm rms) that includes spatial wavelengths smaller than 1 μm. These values have to be realized in order to minimize flare, near angle scattering and wide scattering (outside of the optical system, responsible for a loss of throughput) caused by the MSFR and HSFR, respectively.

In the last few years different ion beam technologies have been developed allowing for form correction and/or shaping of large surfaces with accuracies in the subnanometer depth range and a roughness reduction in the subnanometer range as required in the example mentioned above [28–30].

The main areas of ion beam figuring (IBF) of optical components are the reduction of polishing errors (fine surface figure error) and the production of aspherical wavefront correcting surface figures. During the surface processing with IBF, in the simplest case, an inert gas ion beam of subaperture size and nearly rotationally symmetric Gaussian profile is scanned in a well-controlled manner over the surface of the substrate to be corrected by means of a five-axis motion system in vacuum. On the basis of a surface figure error measured by interferometry for example, the dwell time of the processing beam is varied in a computer-controlled manner according to the amount of material that has to be removed

at each given surface position. As a result, a machining process is defined which converges rapidly within the stated boundaries. No surface contact with the figuring tool in this case implies no weight loading and no edge effects compared to other polishing and figuring techniques. This together with an accurate control of the removal rate results in an efficient correction of long spatial wavelength errors with almost no surface or subsurface damage due to the gentle beam surface interactions. Nevertheless, the small removal rates restrict the IBF technique to being a final processing step for polishing error correction with overall machining depth in the micrometer or submicrometer range only. More sophisticated techniques use multistep scanning schemes combined with dwell time algorithm processing by subaperture ion beams of different sizes in order to achieve an efficient correction of low and mid-spatial frequency surface errors down to the subnanometer amplitude level [30].

IBF processes, where for the given length scales the ion beam is considered as homogeneous with a Gaussian fitted or experimentally measured (ion current density) distribution, are stringently deterministic. In contrast, ion beam induced smoothing of micron and nanometer features is strongly coupled to atomistic processes which are characteristic for the much shorter spatial length scales and are less deterministic. Since the 1970s, in the last century, ion beam smoothing or polishing has been discussed as a potential tool for the improvement of (optical) surfaces for the first time [31–33]. Later, the first direct evidence of ion beam induced surface smoothing was found by Spiller, who used low energy ion bombardment at grazing ion incidence angles to smooth interfaces in the process of deposition of multilayer x-ray mirrors [34]. This technique is now well established for the compensation of growing film roughness during the deposition of multilayers for x-ray optics where the interface roughness is very crucial for the reflectivity of the mirror [35–39]. In the meantime, the benefits of ion beam smoothing have been demonstrated for a lot of further applications such as the reduction of Néel 'orange peel' coupling in magnetic tunnel junctions by smoothing of NiFe films [40] or the conductivity enhancement of ultrathin metal films [41]. Further applications of ion beam smoothing processes for the preparation of ultrasmooth optical surfaces with rms roughness values of $\leqslant$0.1 nm, as required for EUVL components, will be presented in more detail in section 5.

Even though many of the processes involved in ion beam smoothing of surfaces are not completely understood, the examples listed above qualify ion beams as high precision tools for engineering of surface topography with subnanometer accuracy. In this context, it should be emphasized that Taniguchi had already introduced the term nanotechnology, in 1974, in a keynote paper of the International Conference on Production Engineering (ICPE) in Tokyo [42, 43]. Originally, Taniguchi used the word to describe ultraprecision surface finishing of brittle materials such as quartz crystals, silicon and alumina ceramics. With the original Taniguchi curves, showing the achievable accuracy of surface machining techniques, ion beam machining and processing had been pointed out already as among the potential techniques for achieving surfaces with nearly atomistic precision.

In this contribution, we will summarize our work on ion beam smoothing. In detail, we will review and discuss different potential mechanisms responsible for surface smoothing at the nanoscale, which also includes our experimental work on low energy ion beam erosion of various technologically important materials like III/V compound semiconductors, Si and fused silica. Additionally, it will be shown that by implementing experimental conditions, for which surface smoothing dominates, ion beam erosion can be utilized for a well directed reduction of surface roughness of different materials and for the preparation of ultrasmooth surfaces for many other technologically important materials and related applications. By using broad beam ion sources with appropriate beam dimensions (beam diameter larger than the dimension of the workpiece) or suitable process routines (e.g., scanning schemes similar to those used for IBF), large area processing is feasible. Overall, the aim of the paper is to cover the wide range from exploration of basic mechanisms of ion beam driven surface relaxation to specific applications of ion beam smoothing technology in ultraprecision surface processing.

The paper is organized as follows. In section 2, we briefly review potential smoothing processes believed to be responsible for surface relaxation in the low energy regime, especially for materials which are amorphous or become amorphous during the irradiation process. This also includes the linearized, analytical description of surface evolution during low energy ion beam erosion using the power spectral density function (PSD). In section 3 some results will be illustrated and discussed which are aimed at the exploration of the different relaxation mechanisms for the smoothing of different compound semiconductors, silicon and fused silica. In section 4 the (technological) limits of ion beam direct smoothing are briefly addressed and the use of ion beam planarization and sacrificial layers are introduced in order to overcome some of the constraints of ion beam direct smoothing. Finally, in section 5 selected potential applications of ion beam smoothing are shown and developments of technologies integrating all ion beam smoothing methods, especially as regards surface smoothing of some technologically important materials, are illustrated.

2. Processes contributing to surface smoothing and their linearized analytical description

During ion beam sputtering, a variety of surface processes are active that tend to roughen or smooth the surface. In general, ion bombardment of solids initiates the development of atomic recoils and the generation of defects in the bulk and at the surface. Moreover, surface erosion occurs resulting from sputter removal of near surface atoms. The ion arrival and related sputtering events are stochastic in nature and contribute to surface roughening at atomic length scales. In the absence of any surface relaxation processes the stochastic roughening leads to an increase of the rms surface roughness proportional to the square root of the erosion time or, which is equivalent, to the square root of the applied ion fluence. Sigmund [44, 45] has shown, in addition to the stochastic

nature of the sputtering process, that local variations in the erosion rate occur due to a non-uniform energy deposition by the ions when the dimensions of surface features are comparable to the dimension of the zone where the ions deposit their energy. Sigmund demonstrated that the energy deposited in the collision cascades can be, on average, approximated by a Gaussian distribution function where the shape of the deposited energy distribution depends on the respective ion/target combination and, mainly, on the ion energy of the incoming ions. As a direct consequence, the erosion rate is also a function of the local surface curvature and is larger for troughs than for hillocks. This curvature dependent process can result in an amplification of height fluctuations present in the initial surface profile or caused by stochastic fluctuation of the sputtering process. Additionally, some other roughness promoters could contribute to roughening such as seeding and masking by contaminations, preferential sputtering, grain boundary or orientation dependent sputtering in polycrystalline films. All these processes are especially pronounced for many technologically relevant materials, such as metals and compound materials.

In parallel with the sputter generated roughening, a multitude of surface relaxation processes take place mediated by a mass transport along the surface [1]. At appropriate temperatures, surfaces are smoothed via thermally driven surface diffusion, potentially enhanced by an increased defect production caused by the ion bombardment. In addition, ion irradiation generates directed or random fluxes of recoil atoms moving parallel to the surface, which are able to compensate the curvature dependent sputtering or contribute to ballistically motivated surface diffusion process. For amorphous materials or surfaces that are amorphized during ion erosion, defect mediated ion-enhanced viscous flow may also occur.

2.1. The power spectral density approach for modeling of surface evolution

In a (simplified) linear approximation many of the essential features in the surface evolution under ion beam erosion can be described using a stochastic rate equation for the evolution of the surface height profile $h(\vec{x}, t)$, which is similar to the approach used for thin film deposition processes [46]. In this case, the time evolution in reciprocal space is given by

$$\frac{\partial h(\vec{q}, t)}{\partial t} = -h(|\vec{q}|, t)R(q) + \eta(\vec{q}, t) \tag{1}$$

where $R(q)$ can be regarded as a propagation term describing the roughening or smoothing of surface components with wavenumber q (equivalent to a spatial frequency $f = q/2\pi$). η is a temporally and spatially uncorrelated Gaussian noise that mimics the stochastic nature of the sputter events by incoming ions. It is characterized by a zero mean value and $\langle \eta(\vec{q}, t)\eta(\vec{q}', t')\rangle = 2A\delta(\vec{q} - \vec{q}')\delta(t - t')$. The intensity of this sputter noise is determined by the average sputter yield per incoming ion, the atomic volume of the eroded target atoms and by the ion flux. In a generalized form the propagation function $R(q)$ is given by

$$R(q) = \sum_{i=1}^{4} C_i q^i \tag{2}$$

where each term in equation (2) can be assigned to a specific surface roughening or relaxation effect [47–49]. For example, if the $i = 2$ term is used to describe the curvature dependent sputtering [44, 45] and the $i = 4$ term is considered as thermally activated surface diffusion [48, 49], then, neglecting the sputter noise, equation (1) is identical to the Bradley–Harper model for ripple pattern formation [50].

Equation (1) can be easily solved, giving the (angle averaged) power spectral density function (PSD)

$$\mathrm{PSD}(q, t) = \mathrm{PSD}(q, t = 0)\exp(-2R(q)t) + A\frac{1 - \exp(-2R(q)t)}{R(q)} \tag{3}$$

with $\mathrm{PSD}(q, t = 0)$ as the power spectral density of the initial surface at $t = 0$. The rms roughness σ is obtained from the integration of equation (3):

$$\sigma^2(t) = \frac{1}{2\pi}\int_0^\infty q\mathrm{PSD}(q, t)\,\mathrm{d}q. \tag{4}$$

The power spectral density is easily accessible via measurements by different light scattering techniques or from a Fourier analysis of height profiles measured with different imaging techniques such as scanning force microscopy (AFM) and mechanical or optical profilometry, where the upper and lower bandwidth limits of the individual techniques should be noted. From equation (3) it is evident that smoothing of surface components with wavenumber q occurs if $R(q) > 0$. In the case where surface smoothing dominates for all q, the asymptotic solution ($t \to \infty$) of equation (3) is

$$\mathrm{PSD}(q, t \to \infty) = \frac{A}{R(q)} \tag{5}$$

indicating that the minimal achievable surface roughness is determined by the intensity of sputter noise and the strength of the surface relaxation process(es).

In the continuing discussion *ion beam direct smoothing* will be referred to as a process where $R(q) > 0$; this means that surface smoothing arises directly from the ion beam erosion, including related surface relaxation processes caused by the ion beam irradiation. This is different to *ion beam planarization* or *ion beam smoothing with sacrificial layers* where the smoothing is mediated by the deposition and/or the ion beam erosion of the sacrificial layer, which will be addressed in detail later (see section 4).

2.2. Surface relaxation mechanisms in ion beam smoothing

2.2.1. Thermally driven surface diffusion. According to Mullins' approach [48, 49], different thermally activated processes can occur that, driven by a minimization of the surface free energy, can lead to surface relaxation. For common experimental conditions, evaporation/condensation processes and bulk diffusion are not relevant and surface atomic diffusion is the only process operating. In this case, a flux of mobile species is caused by gradients in the local curvature dependent surface chemical potential. Then the associated rate of surface smoothing is

$$\frac{\partial h(q, t)}{\partial t} = -\frac{D_s\gamma\Omega^2 n}{kT}q^4 h(q, t) \tag{6}$$

where D_s is the surface diffusivity of the diffusing species, γ is the surface free energy per unit area, Ω is the atomic volume, n is the surface density of diffusing species, and kT is the thermal energy at temperature T. Here it is assumed that surface anisotropy and surface steps, as present on crystalline surfaces, can be ignored, which is appropriate for amorphous surfaces or surfaces that will be amorphized during the ion erosion. As the surface diffusion is solely thermally driven, as assumed by Bradley and Harper for explaining ripple formation [50], the surface diffusivity is given by $D_s = \exp\{-E_a/kT\}$ with E_a as the activation energy for surface diffusion.

However, for many experimental conditions, for example at room or slightly elevated temperature, ripple formation is not consistent with a purely thermally activated surface relaxation process. For this context, Carter pointed out [1, 51] that for thermal diffusion an ongoing surface smoothing should be observed, even if the ion beam erosion is interrupted or completed. One of the few cases where ripple formation and smoothing are purely thermally initiated has been seen for the generation and the decay of ripple patterns on crystalline Si(001) at temperatures of >650 °C [52–54].

Nevertheless, ion irradiation results in an increased defect generation and, therefore, can enhance the surface diffusivity and concentration of mobile defect species, whereas the surface transport itself is forced by the minimization of the free surface energy again.

2.2.2. Effective ion induced surface diffusion. In order to account also for sputter rippling under athermal conditions, Makeev and Barabasi [55] have shown that, on expanding the surface height contour description to fourth order in its local spatial derivatives, a term in the form

$$\frac{\partial h(q,t)}{\partial t} = -(D_x q_x^4 + D_y q_y^4) h(q,t) \tag{7}$$

contributes to the rate of surface smoothing. The interplay with the second-order process of curvature dependent sputtering can promote ripple production and/or surface smoothing without inclusion of other surface relaxation processes. In fact, this mechanism, named effective ion induced surface diffusion (ESD), describes the preferential erosion of hillocks compared to troughs and is reminiscent of a surface diffusion process ($\propto q^4$), but without mass transport along the surface. The coefficients $D_{x,y}$ can be calculated from the distribution of the deposited energy [55, 56] and are independent of the temperature. In addition, Carter [56] has shown that processes of order higher than fourth have nearly no influence on the surface evolution.

However, it should be noted that the ESD alone, even though the mechanism is always active, cannot account for surface smoothing and/or ripple formation. In general, ripple wavelengths calculated with parameters extracted from characteristic energy distribution functions are too small compared to experimental values, suggesting that further relaxation mechanisms are involved.

2.2.3. Viscous flow. Another potential relaxation process is surface viscous flow [47, 49, 57, 58]. This process is characteristic for amorphous systems and is driven by a Laplace stress, which generates a particle current parallel to the local surface. Depending on the thickness a and the viscosity η of the amorphous layer the associated relaxation rate is

$$\frac{\partial h(q,t)}{\partial t} = -\frac{\gamma}{\eta} q h(q,t) \tag{8}$$

or

$$\frac{\partial h(q,t)}{\partial t} = -\frac{\gamma a^3}{\eta} q^4 h(q,t). \tag{9}$$

According to Orchard [59] the first equation applies if the wavelength of the surface features is much smaller than the thickness of the layer relaxing via radiation induced viscous flow ($qa \gg 1$, bulk viscous flow). The second equation is valid if the viscous flow is only confined to a thin surface layer ($qa < 1$). Both scenarios have been shown to be relevant in low energy ion beam erosion of surfaces [57, 58, 60–64]. Compared to the case for thermally activated viscous flow, the viscosity can be significantly reduced by radiation induced defects leading to strongly increased relaxation rates.

2.2.4. Ballistic transport processes. Carter and Vishnyakov [51] have proposed, in contrast to surface relaxation mechanisms primarily driven by the minimization of the total surface area, ballistic transport processes initiated by the energy and momentum deposition which generate an extra directed flux of surface atoms (ballistic drift) together with a random component (ballistic diffusion). The collisionally induced atomic drift parallel to the sample surface is the result of the momentum deposition process due to the ion impact. Some of the surface atomic recoils are set in motion by collisions, but they cannot surmount the surface energy barrier and, therefore, they remain on the surface and cause mass transport parallel to the surface. The directed flux of such recoils generates a gradient of the atomic transport parallel to the surface and constitutes a normal surface smoothing rate proportional to the second-order spatial derivative (i.e., $\propto q^2$) [51]. Particularly for near normal ion incidence, the mechanism of curvature dependent sputtering can be (over)compensated by ballistic drift, resulting in a net smoothing effect. The additionally random component present in this process can be considered equivalent to collision motivated diffusion process resulting in a surface normal growth (smoothing) rate proportional to the fourth-order spatial derivative of the height profile (i.e., $\propto q^4$). The coefficients of these q^2 and q^4 terms can be calculated from the analysis of the atomic recoils. For instance, for ballistic drift it was shown [51, 65], that the ion incidence angle (α_{ion}) dependent smoothing rate is given by

$$\frac{\partial h(q,t)}{\partial t} = -\frac{J}{N} f(E) d \cos(2\alpha_{ion}) q^2 h(q,t) \tag{10}$$

with ion flux J, solid atomic density N, $f(E)$ as mean number of recoils generated by the impinging ion, and the mean distance d of recoil displacement.

A similar drift process was recently shown to be the main mechanism responsible for the ultrasmoothness of diamond-like carbon coatings prepared by ion assisted thin film deposition methods [20].

2.2.5. Surface smoothing under glancing ion incidence. Sometimes surface smoothing is also observed under ion beam erosion at glancing ion incidence (typically for ion incidence angles of $>80°$ with respect to the normal to the macroscopic surface plane). The smoothing is thought to be caused by a combination of shadowing and enhanced erosion of surface protrusions [66–69]. Thus, initially the smoothing can be dominated by shadowing effects resulting in increased erosion of surface protrusion compared to surface depression. Later, if the surface becomes more and more smooth, the enhanced erosion of small surface protrusions and edges is important. For glancing incidence, most of the ions incident on a nearly perfect plane surface will be reflected at the specular angle, after collisions with surface atoms. This situation changes if the ion impinges near surface steps or similar surface irregularities (e.g., polishing scratches), where the probability of sputtering off atoms from the surface is significantly increased. Indeed, a recent investigation gives clear evidence for the expected high selectivity of step edge sputtering at grazing incidence ion bombardment compared to sputtering from planar and smooth surfaces [70]. Due to the continuous irradiation of the edges, surface steps are swept out and atomically flat surfaces can be prepared, which can be further amplified by the transport processes mentioned above.

2.2.6. Surface gradient dependent sputtering. The evolution of surface topography and roughening at coarser length scales was originally attributed to variations of sputter yield $Y(\theta)$ with the (local) angle of ion incidence θ. With this assumption a complete description of erosion is possible, in which the local surface gradients are the driving force for the evolution of the surface topography ([1] and references therein). This approach also allows the description of surface structures that develop on a finer microscopic scale, with dimensions of some hundreds of nanometers and even less. Here, the smoothing effect originates from the sputtering process itself because the sputtering yield, and hence the local erosion rate, is a function of the orientation of the incident ion flux relative to the surface normal (local ion incidence angle). For example, at normal ion incidence, surface regions inclined to the incident ion beam are eroded faster than a smooth (planar) surface, resulting in a successive lateral shrinkage (protrusions) or expansion (depressions) of surface features which can lead to a net smoothing of the surface. As shown by Carter *et al*, this deterministic or continuum effect tends to erode existing surface protrusions with a high aspect ratio much faster than depressions [71].

2.2.7. Influence of sample rotation. For the sake of completeness, it should be mentioned that the movement of the sample relative to the ion beam influences the evolution of the surface during ion irradiation. Literally, sample rotation is no surface relaxation process in the strictest sense. However, due to the rotation of the sample around its surface normal, the strength of the curvature dependent sputtering can be reduced and the preferred azimuthal direction given by the incident ion beam is lost, thus allowing only isotropic surface structures to appear. The benefit of sample rotation was first realized for thinning of specimens for TEM analysis [72] and, later, for the depth profiling in surface analytical techniques [73]. Moreover, the first direct evidence of surface smoothing induced by rotation was reported by Cirlin *et al* [74] who have observed first ripple formation on a static non-rotating sample, whereas subsequent rotation during erosion resulted in a ripple smoothing. Nevertheless, in many cases sample rotation does not always suppress surface roughening but often the surfaces roughen with a slower rate compared to the case for no sample rotation. With the surface relaxation mechanisms mentioned above, the effect of surface rotation is also included in theoretical examinations [65, 75, 76].

Table 1. Potential surface relaxation mechanisms and the associated wavenumber scaling of the asymptotic power spectral density $\mathrm{PSD}(q, t \to \infty)$. Viscous flow is assumed to be confined to a layer of thickness a.

Mechanism	Asymptotic wavenumber scaling of $\mathrm{PSD}(q, t \to \infty)$
Thermally activated surface diffusion	$\propto q^{-4}$
Effective ion induced surface diffusion	$\propto q^{-4}$
Viscous flow	$\propto q^{-4}$ if $qa < 1$ $\propto q^{-1}$ if $qa \gg 1$
Ballistic drift	$\propto q^{-2}$
Collision motivated diffusion	$\propto q^{-4}$

2.2.8. Summary. In the preceding paragraphs, different surface relaxation processes relevant for low energy ion beam erosion have been reviewed. Some of these mechanisms are related to mass transport along the surface (thermally activated surface diffusion, viscous flow, ballistic transport) whereas others describe the selective removal of atoms from the surface (ESD, gradient dependent sputtering, glancing angle sputtering). As discussed in section 2, for surface smoothing, to some extent, the dominating relaxation process can be identified via the asymptotic wavenumber scaling of the PSD (see equation (5)). Therefore, this section should be completed with a tabulation of surface relaxation mechanisms and their associated wavenumber scaling accessible from the analysis of the (asymptotic) power spectral density (table 1).

3. Ion beam direct smoothing of selected materials

For ion beam erosion of surfaces it is very likely that two or more smoothing processes are effective simultaneously. In our previous work, surface smoothing of various materials (e.g., Si, III–V semiconductors (AlGaAs, Ga(As, P), In(P, As, Sb)), SiC, polycrystalline Cu(In, Ga)(Se, S), metals (Cu, Al), fused silica (SiO_2), and sapphire (Al_2O_3)) has been investigated. From this collection, some examples are selected where it is believed that some characteristic smoothing processes can be addressed individually.

The basic investigations described below are performed with the same experimental setup (ion beam facility) as was described in [6, 77]. In brief, ion beam smoothing was performed in a custom-built ion beam etching system (base

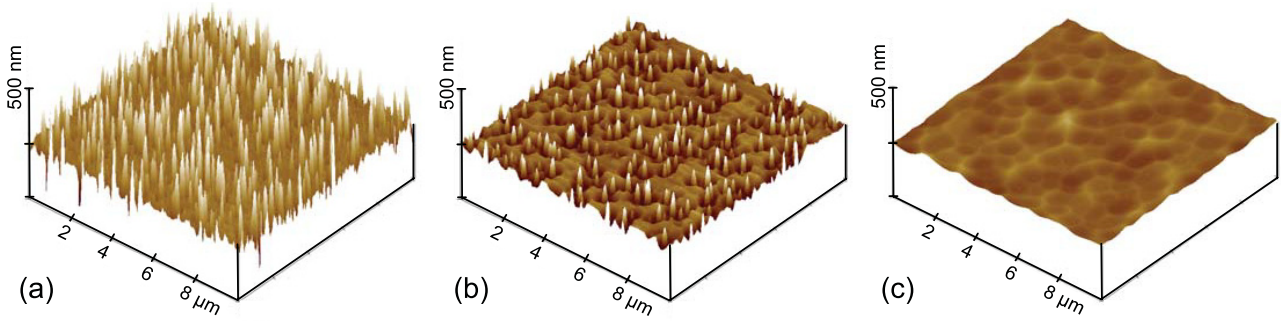

Figure 1. AFM images of temporal evolution of an InSb surface smoothed using N_2^+ ions ($E_{ion} = 500$ eV, normal ion incidence, ion current density 200 μA cm^{-2}) for smoothing times of 10 min (b) and 120 min (c), respectively.

pressure of 1×10^{-6} mbar) using a Kaufman-type broad beam ion source. Samples were mounted on a water-cooled substrate stage. Additionally, the sample stage can be rotated around the surface normal of the mounted sample and the angle of ion beam incidence can be chosen in the range 0°–90° with respect to the surface normal. The ion source used in the experiments was home-built, and the parameters were optimized with respect to well-defined ion energy distributions and small ion beam divergences [78, 79].

For application related ion beam smoothing processes, as summarized in section 5, different in-house ion beam plants equipped with adapted or newly developed ion beam sources and components mature for production requirements have been used [30].

3.1. Smoothing of III/V semiconductor surfaces by surface gradient dependent sputtering

III/V semiconductor materials are well known for their pronounced topographic changes under ion bombardment [12, 13, 80, 81]. In particular, In-containing semiconductors show a pronounced roughness development. In this case indium enrichment, due to the preferential sputtering of for example phosphor, and the surface diffusion of indium are the main mechanisms for the roughness evolution [13]. Because of the different etch rates of indium and the surrounding InP, the small indium islands act as seeding points for the evolution of different surface structures (e.g., cones) during the sputtering process. Under certain circumstances these surface protrusions can arrange into self-organized patterns with different well ordered local arrangements of the individual surface structures [82–84].

However, this surface roughening can be impeded using more reactive ion species, such as nitrogen [85, 86], where the ion beam induced nitridation of a thin surface layer (with a thickness given by the penetration depth of the N^+/N_2^+ ions) inhibits the In agglomeration [87]. In this case, rough surfaces are smoothed by the N_2^+ ion bombardment [88]. An example is shown in figure 1 for an InSb surface (N_2^+ ions, $E_{ion} = 500$ eV, normal ion incidence, ion flux 200 μA cm^{-2}) for smoothing times of 10 min (figure 1(b)) and 120 min (figure 1(c)) corresponding to ion fluences of 0.75×10^{18} cm^{-2} and 9.0×10^{18} cm^{-2}, respectively. The initial surface (figure 1(a)) was pre-roughened by Ar^+ ion beam erosion ($E_{ion} = 500$ eV, normal ion incidence) that allows the reproducible preparation of well-defined rough surfaces by changing the applied Ar^+ fluence [88].

Focusing on protrusions present on the initial surface (figure 1(a)) it is seen from figure 1(b) that the first effect of sputtering is to cause each individual peak to erode downwards. Additionally, a trenching around the cones becomes visible, which is formed by an increase of the local flux due to the reflection of ions on the sidewalls of the cones. If the ion beam erosion proceeds, the cones are completely removed and, finally, the remaining depressions, originating from the trench formation, are leveled out but at a slower rate. This is quantitatively presented in figure 2 showing the time evolution of the rms surface roughness R_q as a function of erosion time for ion incidence angles of 0° (figure 2(a)) and 85° (figure 2(b)), respectively. The experiments for smoothing at 85° were performed with sample rotation.

After a rapid decay of $R_q(t)$ up to an ion fluence $\Phi \sim 4 \times 10^{18}$ cm^{-2}, corresponding to the fluence where nearly all cones are smoothed out, the smoothing slows down for higher ion fluences. In further experiments it has been found that, in the present case, smoothing is especially effective for near normal or grazing ion incidence angles, whereas no or only a reduced smoothing for intermediate ion incidence angles is observed [88]. A similar behavior was found for all semiconductors investigated, such as InP, InAs, AlGaAs and GaP [88–90].

For a discussion of this smoothing behavior, we follow the general description for the evolution of a surface topography under normal incidence ion sputtering (see, e.g., Carter *et al* [1, 91–93]). The normal erosion rate[1] of a surface element m (i.e., velocity parallel to the local surface normal) is related to the sputter yield $Y(\theta)$:

$$-\frac{\partial m}{\partial t} = \frac{JY(\theta)\cos\theta}{N} \tag{11}$$

[1] The erosion rate (or velocity) v is associated with the ion incidence angle dependence of the sputter yield $Y(\theta)$:

$$v(\theta) = \frac{J}{N} Y(\theta)\cos\theta$$

where J is the ion flux measured at normal ion incidence with respect to the macroscopic surface plane, N is the atomic density of the substrate and $\cos\theta$ accounts for the flux correction on a tilted (local) surface.

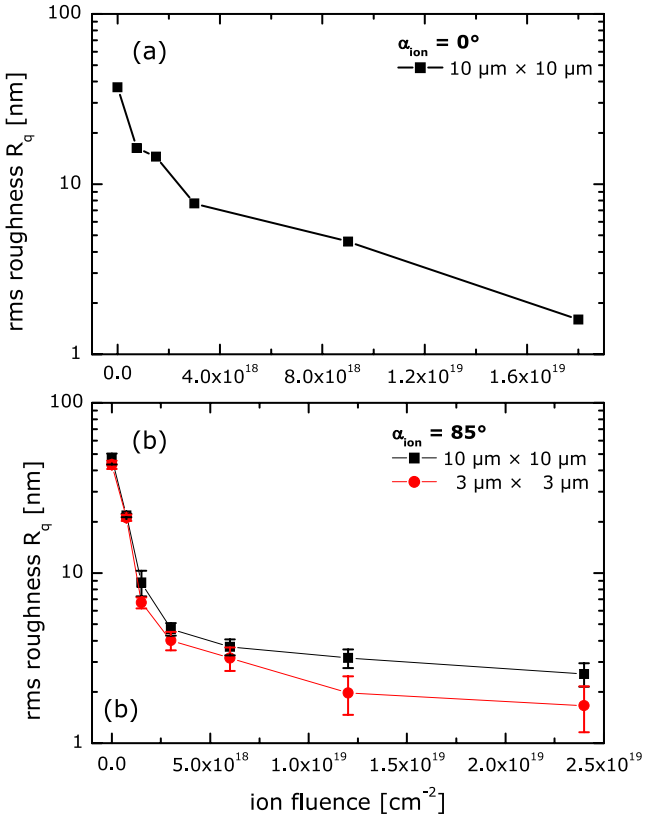

Figure 2. Temporal evolution of rms surface roughness of an InSb surface pre-roughened using Ar^+ and smoothed using N_2^+ ions ($E_{ion} = 500$ eV, ion current density 200 μA cm^{-2}) for ion incidence angles of (a) 0° and (b) 85°. In part (b) rms values for AFM scans of 3 μm × 3 μm are also given, showing the effect of scan size on the roughness determination. Please note the semi-logarithmic scale.

where J is the ion flux measured at normal ion incidence with respect to the macroscopic surface plane, N is the atomic density of the substrate and θ is the angle spanned by the surface normal of m and the incident ion beam. In the case of a one-dimensional surface profile $z(x, t)$ (representing, e.g., a section through a two-dimensional surface profile) the erosion velocities parallel v_x and perpendicular v_z to the surface are given by

$$\left.\frac{\partial x}{\partial t}\right|_\theta = v_x = \frac{J}{N}\frac{\mathrm{d}Y}{\mathrm{d}\theta}\cos^2\theta \tag{12}$$

and

$$\left.\frac{\partial z}{\partial t}\right|_\theta = v_z = \frac{J}{N}\left(\frac{\mathrm{d}Y}{\mathrm{d}\theta}\sin\theta\cos\theta - Y(\theta)\right). \tag{13}$$

An analysis of these equations by Carter *et al* with regard to sputter polishing has shown that surface gradient dependent sputtering, as a matter of principle, results in a smoothing of initially rough surfaces as long as no further roughening precesses are active [71]. They concluded that surface protrusions are eroded very fast compared to troughs with equivalent lateral dimensions, which is confirmed by the data presented in figure 2. In the case of shallow troughs, the small smoothing rates are related to the small surface gradients present in the troughs, as can be concluded from equations (12) and (13). Compared to the erosion velocities of a plane surface ($v_x(\theta = 0) = 0$ and $v_z(\theta = 0) = JY(\theta = 0)/N$), the rates of erosion in the trough (small θ) are only slightly different, which results in a small downwards and inwards motion of the inclined surface elements relative to a plane surface. In contrast, for protrusions, these velocities are large compared to a plane surface resulting in a much more reduced surface roughness for the same smoothing time.

Nevertheless, the following should be mentioned: if further relaxation processes are involved, this might also affect the smoothing behavior. For example, the effect of an additional diffusion process is to prohibit the formation of angular discontinuities. Moreover, it leads to a more rapid attainment of steady state forms and assists or impedes the smoothing of protrusions or depressions, respectively [94].

However, if no further surface transport or erosion mechanisms are involved in the evolution of the surface topography, a thorough analysis of equations (12) and (13) shows that the only possible steady state forms of a surface under ion beam erosion are flat surfaces, normal to the ion flux, and faceted surfaces with semi-vertical angles given by $90° - \theta_p$. For $\theta = \theta_p$ the sputter yield $Y(\theta)$ reaches its maximum [91–93]. The $\pm\theta_p$ faceted surface structures are observed either as planar 'sawtooth' ridges or as collections of cones. In contrast, a combination of planar and faceted surface areas is not a steady state surface form [93] and isolated cones on a flat surface are only transient features; otherwise the whole surface must be cone covered as a permanent surface structure.

The first case is in line to the scenario described here for the smoothing; the other one seems to be relevant for the formation of self-organized dot pattern on III/V compound semiconductor surfaces under inert gas (e.g., Ar^+) ion beam erosion. Dot formation in this case is quite different from the dot and ripple pattern on Si or Ge. Thus, the height of dots formed on InP or GaSb is an order of magnitude higher than that of ones formed on Si and, often, the dots have a cone-like shape [82–84]. The formation of such close packed ordered surface cones might be a clear indication that the evolution of surface features with dimensions even less than 100 nm are affected by first-order erosion effects related to surface gradient dependent sputtering. Further, erosion rates of III/V semiconductor surfaces are, usually, larger compared to those for Si or Ge, which can shift the kinetics of structure evolution towards a more sputter dominated regime. One should take note that the dimensions of collision cascades giving rise to high order effects are still significantly smaller than the dimension of the cones itself. However, for the atomic length scale gradient dependent sputtering has also been discussed as potentially relevant for surface relaxation [95].

3.2. Smoothing of Si surfaces

For ion beam erosion of Si a diversity of surface topographies and patterns can occur, depending on sputtering conditions. In order to illustrate the complex relationships between the different parameters and the related surface patterns, so-called topography diagrams can be used [77, 96]. From these topography diagrams, as regards E_{ion} and α_{ion}, three different regions can be distinguished. In the first region, extending

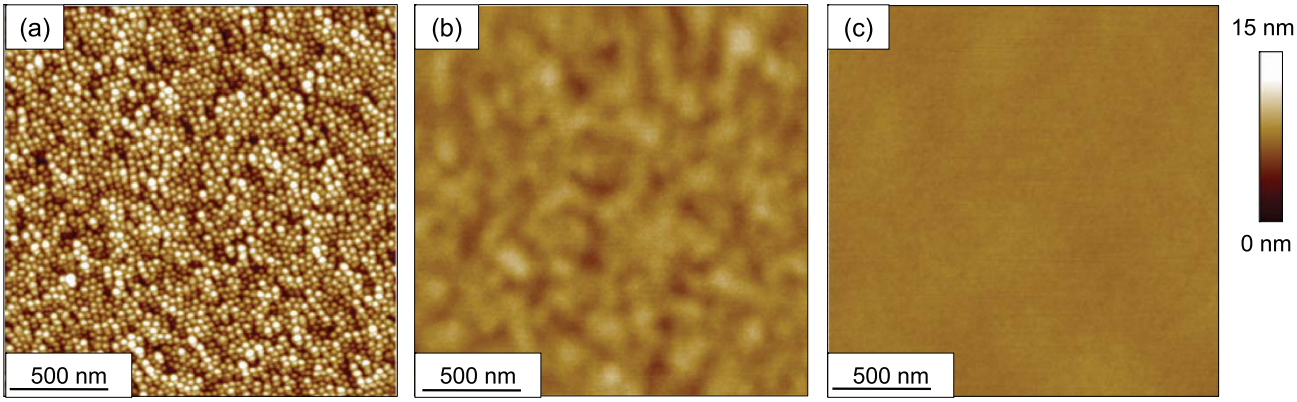

Figure 3. Sequence of AFM images which shows the progressive smoothing of a Si surface under Ar^+ ion beam erosion ($E_{ion} = 500$ eV, $\alpha_{ion} = 45°$, $j_{ion} = 300\ \mu A\ cm^{-2}$, simultaneous sample rotation). (a) Initial surface (pre-roughened by Ar^+ erosion at 75° ion incidence), (b) after 10 min (corresponding to a total applied ion fluence of $\Phi = 1.1 \times 10^{18}\ cm^{-2}$) and (c) after 180 min ($\Phi = 2.0 \times 10^{19}\ cm^{-2}$). The rms roughness was reduced from $R_q = 2.25$ nm to $R_q < 0.2$ nm.

from normal up to ∼30° ion incidence, patterns develop on the surface, with the exception of when ion energies are intermediate (approximately 900–1200 eV). For ion incidence angles between ∼35° and ∼60° the surface remains smooth, nearly independent of the ion energy and ion species used for the experiments. For these ion incidence angles, the surfaces are stable against ion beam induced roughening. Finally, for ion incidence angles of approximately 65° and 85°, the surface roughens again and pronounced topographical changes are observed.

In the context of ion beam smoothing, the windows of stability are especially important; this means parameter regimes where surface relaxation dominates. Applying now ion beams with appropriate values of E_{ion} and α_{ion} on initially rough surfaces, a smoothing is expected. This is illustrated in figure 3 showing AFM images for the initial surface before smoothing ($t = 0$ min) and after smoothing times of $t =$ 10 min and 180 min, respectively. The successive surface smoothing is evident and the rms roughness was reduced from $R_q = 2.25$ nm at $t = 0$ min to $R_q < 0.2$ nm at $t = 180$ min.

For a detailed study of the relevant surface relaxation mechanisms, systematic investigations of the smoothing of Si surfaces have been conducted. In particular, the time evolution of the power spectral density (PSD) and the rms surface roughness were analyzed. For the given case the time evolution of the power spectral densities $\mathrm{PSD}(f, t)$ and the rms roughness $R_q(t)$ during ion beam smoothing are summarized in figure 4. Starting from the PSD of the initial surface $\mathrm{PSD}(f, t = 0)$, first a rapid decrease of the small spatial wavelength (large frequency) surface features is observed and finally a steady state is reached also for lower frequencies by a successive smoothing of larger length scale features. In this steady state the PSD growths according to a power law: $\mathrm{PSD}(f = q/2\pi, t) \propto q^{-2}$. The q^{-2} behavior is confirmed by an analysis of the set of $\mathrm{PSD}(f, t)$ curves using equations (2) and (3) where the values $C_2 = 1.83\ nm^2\ s^{-1}$, $A = 0.05\ nm^4\ s^{-1}$, and $C_1 = C_3 = C_4 = 0$ were determined. Consequentially, using these values and equation (4) for the calculation of $R_q(t)$ this yields an excellent agreement with the measured roughness values. The small deviation from q^{-2} behavior in the PSD curves at large q is caused by the noise present in the AFM measurements.

From the list of surface relaxation mechanisms reviewed in section 2, the only surface relaxation process which is consistent with the experimental results is a collisionally induced atomic drift process parallel to the sample surface. According to Carter and Vishnyakov [51] the related smoothing rate is $C_2 \propto \cos(2\alpha_{ion})$ (see section 2.2.4) which implies no additional smoothing effect at the ion incidence angle used in our experiments. However, in their analysis, Carter and Vishnyakov considered only parallel mode ripples (i.e. ripples with a wavevector parallel to the ion beam projection), which are typically expected for near normal ion incidence. Therefore, solely the ion induced ballistic flux along the projection of the ion beam was included. As recently pointed out by Davidovitch *et al* [97], for a surface $h(x, y)$ there is also a flux component perpendicular to this direction, similar to the two modes for curvature dependent sputtering. Using the expression for the ion induced ballistic drift contribution parallel and perpendicular to the ion beam direction as derived in [97], it can be easily shown that in the given case of simultaneous sample rotation, the averaged strength of the smoothing is a continuously decreasing function of the ion incidence angle with a maximum at normal incidence and a value of zero at the ion incidence of 90°. Consequently, for all ion incidence angles an effect of stabilizing or smoothing by the ballistic process is operative, including for 45° ion incidence.

The importance of ballistic drift mechanisms has also been emphasized by Vauth and Mayr [63], studying the relevance of surface viscous flow, surface diffusion, and ballistic drift effects for the ion beam smoothing of amorphous surfaces at room temperature in the keV ion energy range. Using a multiscale modeling (a combination of molecular dynamics with continuum approaches), they show that surface diffusion is less important. In contrast, viscous flow or ballistic drift is dominant, depending on the size of the surface structures. For the simulated scenario of 1 keV Si^+ on a-Si at $\alpha_{ion} =$

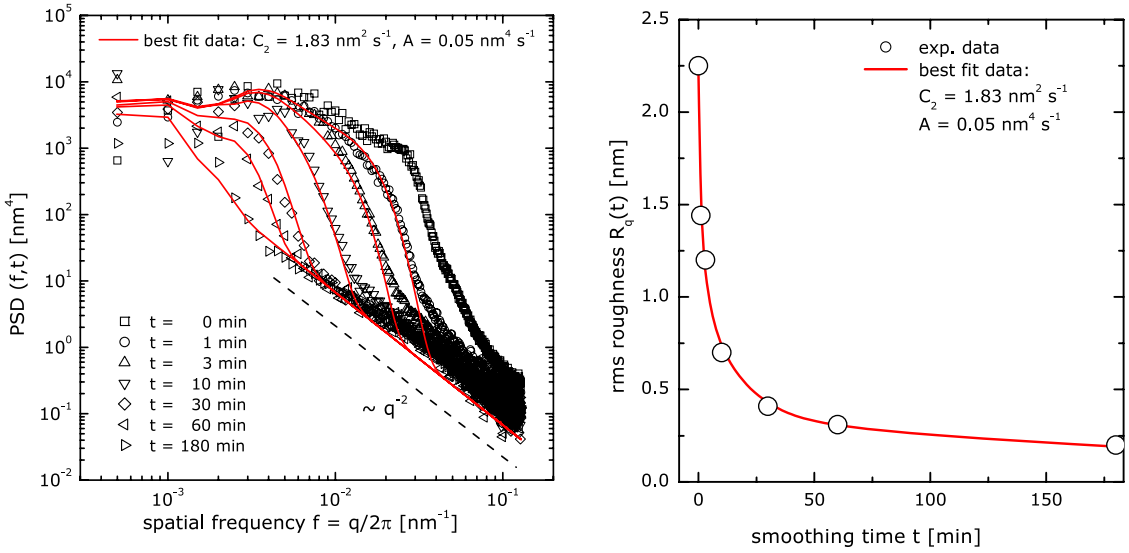

Figure 4. Power spectral densities (left) and rms surface roughness R_q (right) for different smoothing times calculated from 3 μm × 3 μm AFM measurements (see figure 3). The solid line PSD curves were obtained from curve fitting analysis using equation (3) with values as indicated ($C_1 = C_3 = C_4 = 0$; see equation (2)). The dashed line presents a power law scaling: PSD(q) $\propto q^{-2}$. The solid line for $R_q(t)$ was estimated from equation (4) using the values of C_2 and A from the PSD analysis.

45°, Vauth and Mayr estimated a transition from ballistic drift dominated smoothing at larger spatial wavelength to viscous flow mediated smoothing for smaller spatial wavelength with a transition wavelength between 40 and 25 nm, depending on simulation details. Indeed we have found first evidence for a transition from a ballistic drift mediated smoothing ($\propto q^{-2}$) to a viscous flow ($\propto q^{-4}$) dominated situation. Due to the inclusion of AFM measurement with smaller scan sizes the noise present in figure 4, especially along the slow scan axis, is shifted to higher spatial frequencies and a transition from a q^{-2} to a q^{-4} behavior at a spatial wavelength of approximately 30 nm was observed (figure 5).

From the preceding discussion, it is reasonable to consider ballistic drift as a dominating surface relaxation mechanism in low energy ion smoothing erosion of Si surfaces. Nevertheless some experimental observations suggest that ballistic drift mechanisms alone cannot account for all of the experimental findings.

For example, analyzing the curvature dependent Bradley–Harper coefficients $\Gamma_x(\alpha_{\text{ion}})$ and $\Gamma_y(\alpha_{\text{ion}})$ it can be found that they change only slightly if the ion incidence angle goes from oblique angles ($\alpha_{\text{ion}} \leqslant 45°$) to normal incidence. In contrast the ballistic drift coefficients increase much more with decreasing ion incidence angle until they reach their maximum value for normal incidence. Hence, it is expected that the relaxation times (smoothing rates) for identical initial surfaces should be smaller (higher) for normal incidence compared to oblique ion incidence. Indeed we found that using the same smoothing conditions as discussed above (Ar^+, $E_{\text{ion}} =$ 500 eV, $j_{\text{ion}} = 300$ μA cm^{-2}) but for normal ion incidence the surface smooths considerably faster compared to the case for normal incidence. However, after a short transient phase of smoothing the surface roughens again and the topography seen in figure 3(a) changes to a surface consisting of holes, which coalesce and become larger with increasing erosion time. This surface topography is very reminiscent of surfaces obtained in the simulation of plasma etching and reactive ion etching processes using a so-called flux redistribution model [98]. This model can be adapted to ion beam eroded surfaces if backscattered projectile ions and highly energetic sputtered Si atoms are considered as redistributed particles [99]. Within detailed TRIM.SP simulations [100] it was shown that these energetic species can generate secondary sputter events, impeding the growth of surface features with higher amplitudes. This stabilizing process can also provide

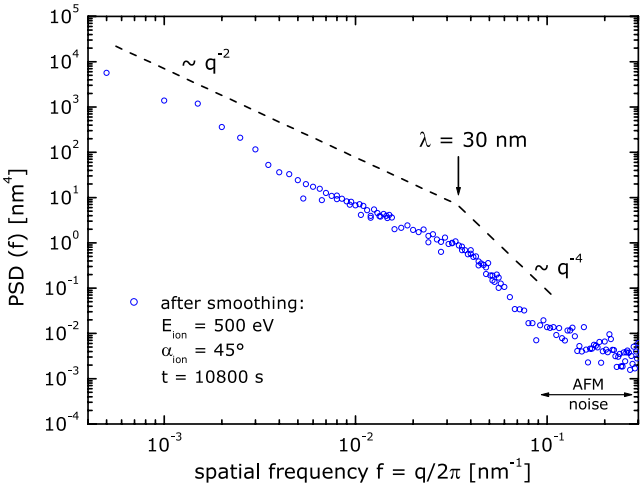

Figure 5. Power spectral density curve of an ion beam smoothed Si surface (Ar^+, $E_{\text{ion}} = 500$ eV, $\alpha_{\text{ion}} = 45°$, $j_{\text{ion}} = 300$ μA cm^{-2}, $t = 10\,800$ s) pieced together from AFM measurements with different scan sizes. The dashed lines show power law scalings with PSD(q) $\propto q^{-2}$ and PSD(q) $\propto q^{-4}$. The transition from a q^{-2} to a q^{-4} behavior at a spatial wavelength of approximately 30 nm is indicated. Please note that the high spatial frequency range of the PSD ($f > 0.1$ nm^{-1}) is dominated by AFM measurement noise.

an alternative explanation of the damping term proposed by Facsko *et al* [101] to reproduce the long range order in simulations of self-organized pattern formation by ion beam erosion. We defer a more detailed discussion of the overall results to a later date [99].

To conclude this paragraph, the summary of investigations of the smoothing behavior presented has shown that (i) detailed studies of smoothing processes can give very useful insights into processes also relevant for pattern formation, (ii) for low energy ion beam erosion of Si surfaces ballistic drift (i.e., atomic transport parallel to surface) plays an important role, (iii) ballistic drift overcompensates for curvature dependent sputtering for normal and near normal ion incidence, (iv) potentially viscous flow becomes important for high spatial frequency roughness components, (v) using TRIM.SP simulation the first evidence was found for the importance of secondary sputter effects caused by backscattered projectile ions and sputtered Si on the topography evolution during low energy ion beam erosion.

3.3. Smoothing of quartz glass

Motivated by the technological interest, we have conducted considerable amounts of work in efforts to shed light on the topography evolution of quartz glass surfaces under low energy ion beam erosion [102, 103]. Briefly, it was found that, depending on the incidence angle, different surface topographies emerge. For ion incidence angles less than a critical angle, surface smoothing is observed. Beyond this critical incidence angle, ripple structures with a characteristic wavelength λ between 30 and 300 nm form. Their wavelength increases with ion energy but it is constant with respect to the ion flux. As regards the kinetics of surface topography, power law scaling relations for the surface roughness $R_q \sim t^{\beta}$ and ripple wavelength $\lambda \sim t^{\gamma}$ were found, where the scaling exponents β and γ are determined by the ion beam parameters [102, 103]. Important results of these studies (e.g., ripple coarsening) are also confirmed for glass surfaces by other groups but without specifying the exact type of glass which was used [104]. In contrast, no ripple coarsening was seen on SiO_2 surfaces conventionally wet oxidized from Si surfaces where ion-enhanced viscous flow is proposed as a potential relaxation process [58]. However, in our work no clear indication of one of the surface relaxation processes listed in section 2 has been found until now [110, 113].

Nevertheless, from an application oriented point of view it is most notable that, as in the case of Si, a window of stability exists where surface relaxation dominates, which can be implemented in technological processes for smoothing of optical elements. Thus, ion beam smoothing of technologically relevant quartz glass surface down to 0.1 nm rms roughness values could be demonstrated [29, 113].

As briefly explained above, for the case of non-rotating samples, for ion incidence angles larger than a critical angle, ripple structures emerge on quartz surfaces. This critical angle is found to be in the range between 40° and 45°. Therefore for sputtering at $\alpha_{\text{ion}} = 50°$ ($E_{\text{ion}} = 800$ eV, $j_{\text{ion}} = 400\ \mu\text{A cm}^{-2}$), parallel mode ripple structures are formed. The ripple wavelength increases with erosion time from $\lambda = 50$ nm at 3 min to $\lambda = 145$ nm for 240 min. Simultaneously the ripple amplitude grows and, hence, the surface roughness rises. The temporal increase of surface roughness with erosion time is shown in figure 6 and can be described with a power law scaling $R_q \sim t^{\beta}$ with $\beta = 0.57 \pm 0.02$. The situation changes completely if the sample rotates during erosion at 12 min^{-1}. Then the roughness reduces slightly with erosion time as indicated by a negative value for $\beta = -0.08 \pm 0.03$ in figure 6. From a PSD analysis, surface smoothing for all spatial frequencies is evident and, therefore, from equations (2) and (3) it can be seen that $R_{\text{rot}}(q) > 0\ \forall q$ whereas $R_{\text{static}}(q) < 0$ at least for an interval of values of q corresponding to the ripple wavelength. For curvature dependent sputtering alone it can be easily calculated that $R_{\text{static}}(q) - R_{\text{rot}}(q) \propto 1/2(\Gamma_x(\alpha_{\text{ion}}) - \Gamma_y(\alpha_{\text{ion}})) < 0$ because $\Gamma_x(\alpha_{\text{ion}}) < \Gamma_y(\alpha_{\text{ion}}) < 0$. Therefore the surface destabilization by curvature dependent sputtering is significantly reduced due to the simultaneous sample rotation [75]. In addition, ballistic smoothing mechanisms (or, in general, all non-isotropic smoothing mechanisms) can be amplified by the rotation, as discussed for ballistic drift smoothing of Si surfaces (see section 3.2).

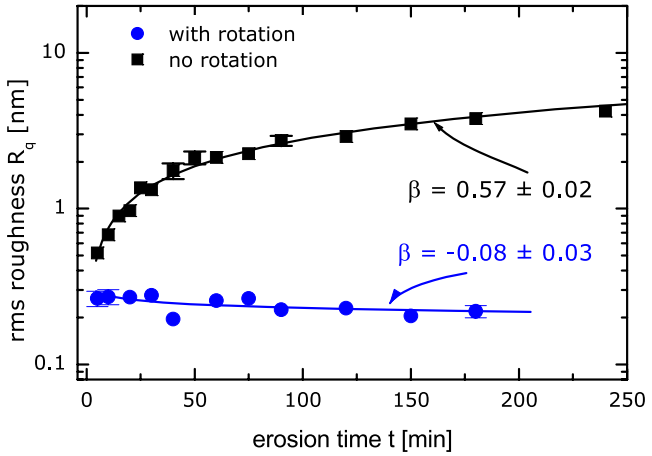

Figure 6. Time evolution of the rms surface roughness R_q for ion beam erosion of a fused silica surface at $\alpha_{\text{ion}} = 50°$. The squares refer to the case of a static sample (ripples are formed) and the circles correspond to the case of simultaneous sample rotation ($E_{\text{ion}} = 800$ eV, $j_{\text{ion}} = 400\ \mu\text{A}^{-2}$). The lines represent the fits according to a power law scaling relation $R_q \sim t^{\beta}$. The values of β obtained are given in the figure. A negative value for β corresponds to a surface smoothing. The error bars plotted for R_q are given by the standard deviation obtained from various experimental sputter runs.

4. Ion beam planarization and ion beam smoothing with sacrificial layers

4.1. Constraints in ion beam direct smoothing

In section 3, surface smoothing by ion erosion mediated relaxation mechanisms has been illustrated and discussed. Ion beam direct smoothing is possible for a multitude of materials in addition to the example materials—for example SiC and GaN—emphasizing the relevance of this technique as a process for the preparation of ultrasmooth surfaces.

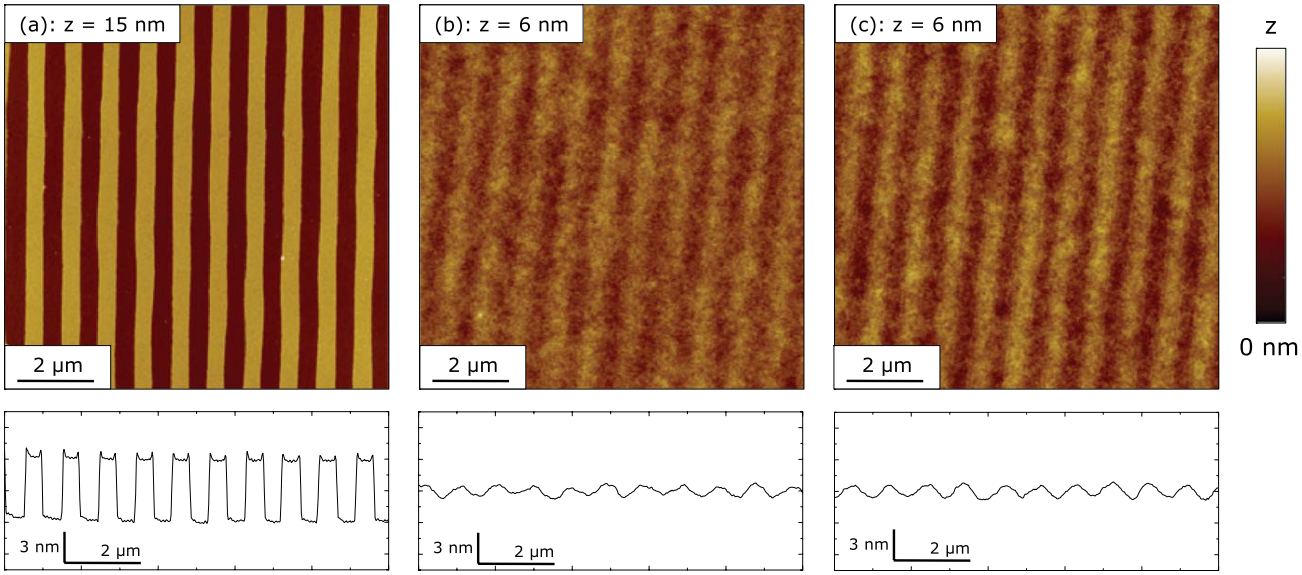

Figure 7. Demonstration of the ion beam planarization technique for an artificial Si surface. (a) Binary grating with periodicity of 950 nm in Si ($R_q = 3.05$ nm), (b) resist surface after coating the Si surface shown in (a) with a 55 nm thick planarizing photoresist layer ($R_q = 0.45$ nm), (c) Si surface after ion beam erosion of the planarizing film together with the rough Si structure to a depth below the bottom of the Si groove structure ($R_q = 0.60$ nm). The characteristic section profiles were obtained from the AFM images by averaging over 20 scan lines. Please note the different height scales of the AFM images.

However, for a practical implementation of this technique some constraints exist, which should be briefly addressed. Using the simplified linear description as given in section 2, the smoothing occurs if $R(q) > 0$ and the respective smoothing rate is related to the (dominating) atomistic relaxation processes by $R(q) \propto C_i q^i$. Therefore, the smoothing rates decrease for decreasing q, which slows down the smoothing of larger length scale structures, regardless of the dominating surface transport process. This can also be seen from figure 4 for the ballistic drift smoothing of Si surfaces where the amplitudes of surface components with $f < 10^{-2}$ nm^{-1} are significantly reduced only for smoothing times of >30 min.

In addition, if we consider surface smoothing by gradient dependent sputtering, it has been shown (figure 2) that the initially present protrusions are smoothed very effectively, whereas remaining depressions are smoothed at a considerably slower rate. Using a simplified analysis, Carter *et al* [71] have pointed out that most of surface asperities may be eroded by sputtering a depth equivalent to several average wavelengths between surface asperities, whereas very fine polishing of the depressions requires a depth erosion equivalent to hundreds to thousands of trough wavelengths. Both examples show that in the case of ion beam smoothing of long wavelength structures, especially with small amplitudes, long processing times are required.

Finally, it should be mentioned that ion beam direct smoothing of certain, especially technologically important, materials has proved to be particularly problematic. Polycrystalline metals, composites and ceramic materials belong to this category, where the different sputtering yields of the constituent parts are thought to be a catalyst for the roughness evolution.

In the following, alternative approaches used to overcome some of these drawbacks will be discussed.

4.2. Ion beam planarization

An alternative process for surface smoothing is the so-called ion beam planarization technique. Within the planarization technique, smoothing results from removal of a planarizing sacrificial layer, as commonly used in semiconductor technology for the planarization of processed silicon wafers. For the smoothing of optical surfaces this process was originally proposed by Johnson and Ingersoll [105, 106] and further developed by Fechner *et al* [107].

Usually, thin photoresist planarizing layers are applied onto the rough substrate either by spin coating or by spray coating. Subsequently the sacrificial layer is removed by ion beam sputtering at the planarization angle (i.e., at an angle where the removal rates of the resist and the underlying substrate are nearly identical). Thus, the smooth surface of the sacrificial layer is transferred to the substrate if the ion beam erosion step does not cause an additional roughening of the planarizing layer. Small deviations from the ideal planarization angle are tolerable.

The process is illustrated in figures 7 and 8 for an artificially roughened Si surface. The initial surface (a) was a binary grating etched into Si with a periodicity of 950 nm and an rms roughness of $R_q = 3.05$ nm, according to the etch depth. In the first step the surface was coated with a 55 nm thick photoresist layer, whereby the surface roughness is reduced to $R_q = 0.45$ nm. Finally, the resist layer was removed by the ion planarization step, resulting in surface (c) with $R_q = 0.60$ nm. The small differences between the amplitudes on the resist and Si surface might be caused by deviations from the ideal planarization angle. The leveling of surface steps by the resist layer as well as the reduced profile height in the final Si surface are also evident from the characteristic section profiles shown in figure 7 and from the PSD curves

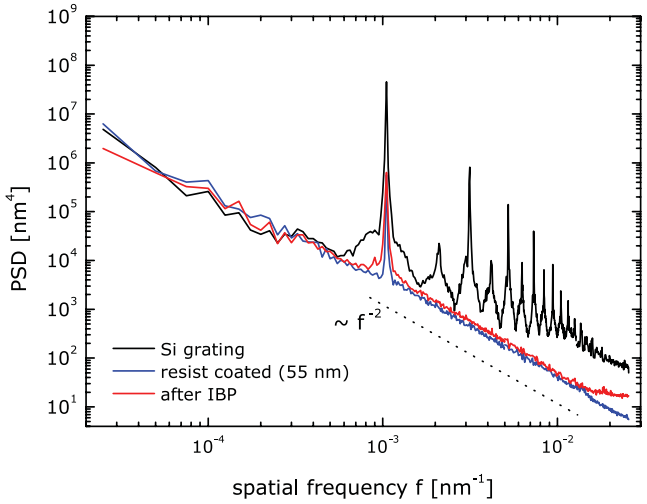

Figure 8. Power spectral density curves from the AFM images in figure 7. The dashed line shows power law scaling according to PSD(q) $\propto q^{-2}$. The characteristic peaks correspond to the grating period of 950 nm.

displayed in figure 8. Surprisingly, for the resist coated surface a PSD(q) $\propto q^{-2}$ has been observed. A similar dependence is found for using a polyimide as the smoothing agent [108]. For a viscous flow related smoothing process (see section 2.2.3) usually a PSD(q) $\propto q^{-4}$ behavior is expected, because the product of the grating wavevector $q_0 = 2\pi/950$ nm and the resist film thickness $d = 55$ nm is <1.

This modified smoothing behavior can possibly be explained by the evaporation of the solvent out of the resist during the coating. As shown for the leveling of paints [109], the evaporation of the solvent may give rise to the development of surface tension gradients along the surface, resulting in a modified smoothing rate $R(q) \propto q^{-2}$. In contrast, Orchard assumed a constant surface tension [59].

In general, the example clearly demonstrates that ion beam planarization is very efficient for smoothing of long wavelength surface structures.

4.3. Ion beam direct smoothing versus ion beam planarization

For a direct comparison between ion beam direct smoothing and ion beam planarization, surfaces with different roughness spectra and surface structure have been used [110]. Therefore, Si wafer surfaces were deliberately roughened under unfavorable ion beam erosion conditions, whereby holes as well as dot structures are generated (see the insets in figure 9). The two samples are denoted as test sample 1 (dot-like surface structures, similar to the surface used for the experiments in section 3.2) and test sample 2 (hole-like structured surface) with initial surface roughnesses of $R_q = 2.1$ nm and $R_q = 1.7$ nm, respectively. Subsequently, different pieces of both wafers were subjected to the same ion beam direct smoothing process (Ar^+, $E_{ion} = 500$ eV, $\alpha_{ion} = 45°$, $j_{ion} = 300$ μA cm^{-2}, simultaneous sample rotation) but for different smoothing times. The time dependences of the ion beam direct smoothings for the two test samples are summarized in figure 9. The degrees of roughness reduction caused by the ion beam smoothing are rather different for the two surfaces. While the small dot-like asperities completely disappeared for a smoothing time of 10 min, the hole-like depressions are still obvious in the AFM images (not shown). This is also confirmed by rms values of $R_q = 0.4$ nm and $R_q = 1.1$ nm for the two surfaces (figure 9). This difference in smoothing behavior is due to the various portions of high spatial frequency and low spatial frequency surface wavelengths which determine the efficiency of the ion beam smoothing process. As outlined in section 4.1, surface irregularities with high spatial frequencies have a higher smoothing rate, while low spatial frequency components require longer sputter times.

However, it should be noted that for both surfaces a final state rms roughness below 0.2 nm is obtained, which is equivalent to the rms value after long time sputtering of an unprocessed initially smooth wafer. For comparison with ion beam planarization, experiments were conducted where both Si model surfaces have been coated with a thin photoresist layer. Then the resist was removed by an Ar^+ ion beam planarization step (with the same conditions as were used for the direct smoothing). After removal of the resist, the uncovered Si surface was sputtered for another 10 min (overetching) to promote the effect of the ion beam direct smoothing. The rms roughness was measured as $R_q \sim 0.4$ nm and $R_q \sim 0.5$ nm. Whereas the roughness obtained for the dot-like structured surface is comparable to that for ion beam direct smoothing without adding the planarization step, the roughness for the hole-like structured surface was significantly improved as compared to that for ion beam direct smoothing alone (solid circles in figure 9). The results can be attributed to the enhanced smoothing of low spatial frequency surface features. As regards the dot-like Si model surface, the two processes, ion beam direct smoothing and the planarization technique, are equivalent and no additional planarization step is necessary. However, for the hole-like Si model surface containing more low spatial frequency surface wavelength structures, an additional planarization step is essential.

This comparison shows that the combination of the two techniques offers subnanometer scale roughness reduction covering a broad range of spatial wavelength structures.

4.4. Ion beam smoothing with sacrificial layers

For some, especially technologically important, materials, ion beam smoothing does not work and ion beam erosion, regardless of the processing conditions, results in increased surface roughness even after removal of only very thin surface layers. This is also problematic as regards possible overetching effects in ion beam planarization, whereby an additional roughness can be generated. In these cases, it might be beneficial to shift the process of ion beam smoothing to a thin sacrificial layer deposited on the substrate which has to be smoothed. According to the discussion of ion beam direct smoothing, potential sacrificial layers are, for instance, Si or SiO_2. The films are smoothed (and removed) except for a thin residual layer. A basic requirement for the utilization of this process is that the residual layer does not affect the later

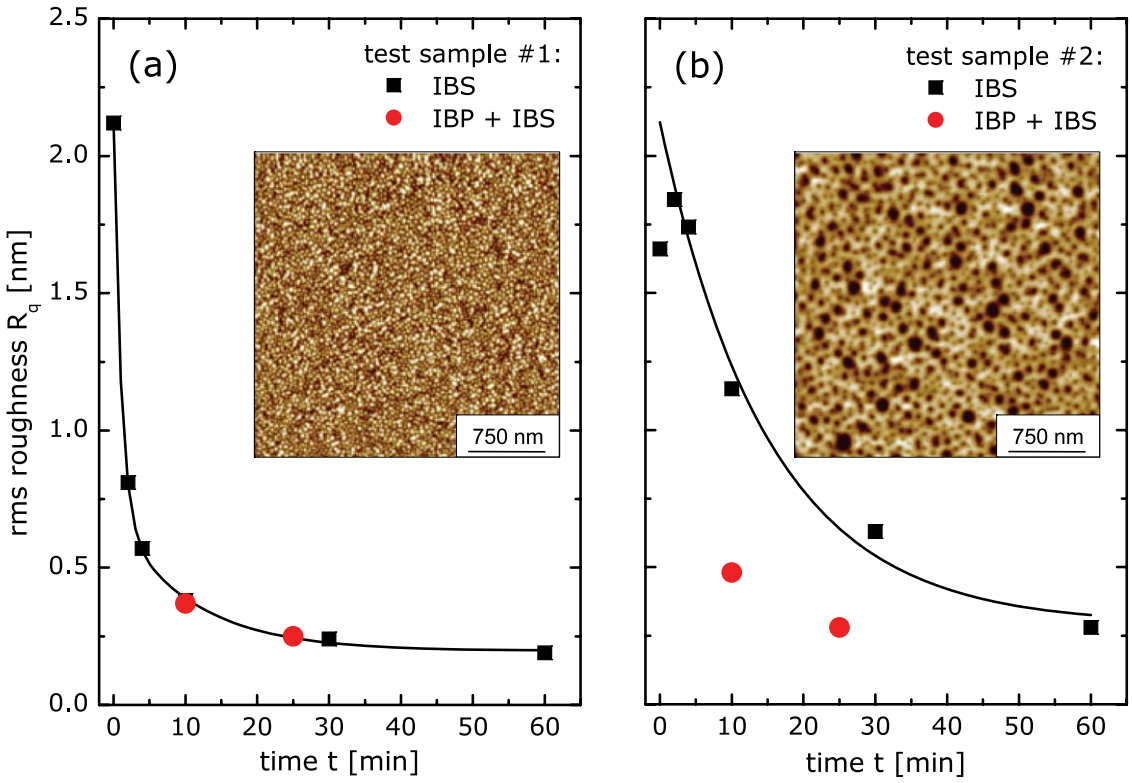

Figure 9. Comparison of ion beam direct smoothing and ion beam planarization, for two different Si test samples: (a) test sample 1: dot-like structured surface (AFM image in the inset); (b) test sample 2: surface with small depressions as shown in the inset. The solid squares refer to the ion beam direct smoothing of the surfaces with increasing erosion time (Ar^+, $E_{ion} = 500$ eV, $\alpha_{ion} = 45°$, $j_{ion} = 300\ \mu$A cm^{-2}, simultaneous sample rotation). The solid circles give the roughness values for the two test samples obtained with ion beam direct smoothing times of 10 and 25 min, but with an intermediate planarization step. The solid lines are calculated using the same values for C_2 and A as were determined in section 3.2 for these ion beam smoothing conditions.

device or component performance. A specific example for this approach will be shown later for the smoothing of Zerodur® substrates (see section 5.2).

5. Applications of ion beam assisted smoothing

In the preceding sections, low energy ion beams emerge as an alternative tool that can be beneficially used to tailor the microscopic surface roughness of solid surfaces on nanometer and micron spatial wavelength scales. In this section, we will focus on recently developed different ion beam assisted processes for the preparation of ultrasmooth surfaces. In particular, ion beam direct smoothing, but also in combination with ion beam planarization and/or sacrificial layer smoothing, will be demonstrated. The ion beam assisted smoothing techniques were investigated for a wide range of various materials and examples are given here for the ion beam direct smoothing of Si substrates as used for synchrotron optics, the smoothing of Zerodur® mask blanks for the EUV lithography and the removal of tool marks from NiP surfaces originating from single-point diamond turning.

5.1. Ion beam direct smoothing of synchrotron optics

To demonstrate the capabilities of ion beams for surface smoothing, in figure 10 the results of the processing of a Si substrate as used for synchrotron optics, where surface roughness is a critical issue, are illustrated [111]. In the AFM images (a) and (c), 1 and 10 μm scans of a magnetorheological finishing (MRF) processed Si substrate are shown. Both images show pronounced rather coarse-grained tool marks together with a superimposed additional fine structure (corresponding to the shoulder found in PSD curves at $f \sim 0.02\ \text{nm}^{-1}$; see figure 10(e)) and contaminations resulting in an overall degradation of the surface roughness. After an ion beam direct smoothing step, both the tool marks and the contaminations are significantly removed and the surface roughness is reduced to rms values of 0.2 nm and 0.43 nm for measuring areas of $(1\ \mu\text{m})^2$ and $(10\ \mu\text{m})^2$, respectively. The PSD curve in (e), calculated from the $1 \times 1\ \mu\text{m}^2$ and $10 \times 10\ \mu\text{m}^2$ scans, indicates a surface smoothing for all spatial wavelength components covered by the AFM measurements. As expected, from the PSD graph it can be recognized that surface smoothing is less pronounced for larger spatial wavelength features due to the reduced smoothing rates ($R(q) \propto C_2 q^2$) of the ballistic drift process for small q values.

Nevertheless, the physical constraints can be relaxed with the help of further ion beam assisted smoothing techniques, as will shown in the following examples.

5.2. Smoothing of Zerodur® substrates for EUVL mask blanks

Today, the most stringent conditions as regards the accuracy and smoothness of surfaces are imposed on optical compo-

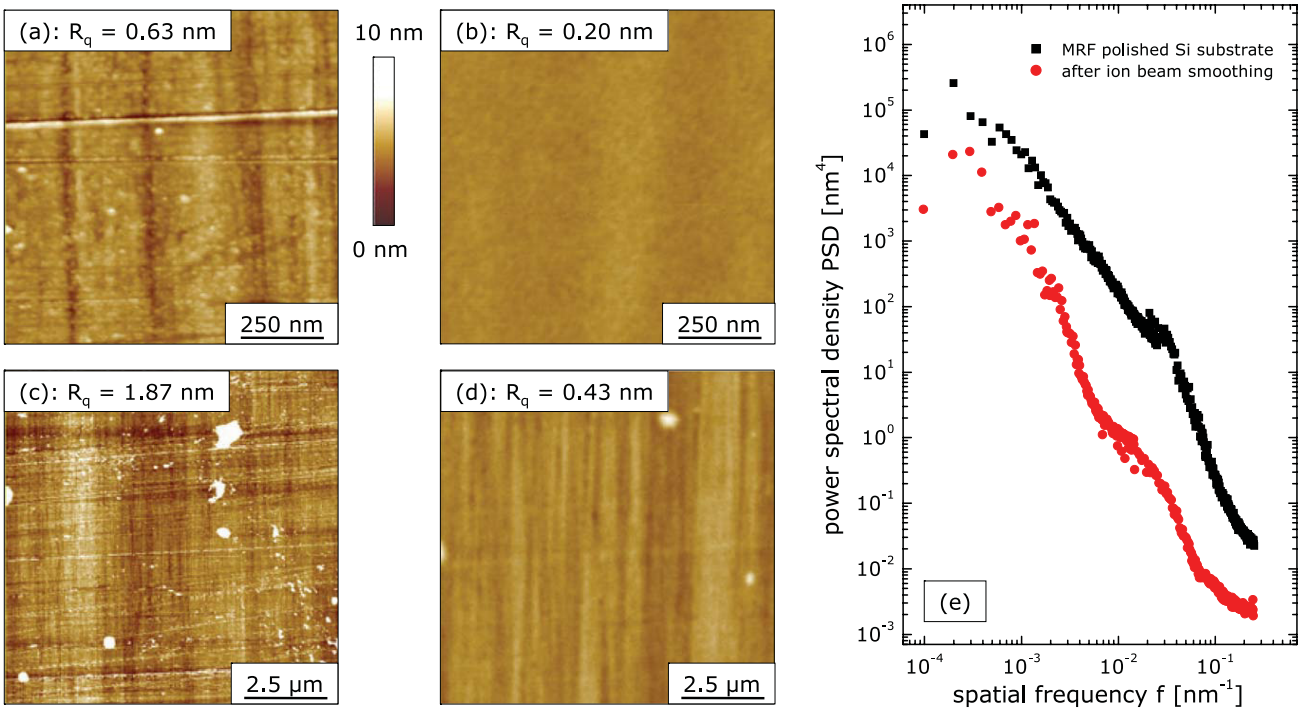

Figure 10. Ion beam direct smoothing of a Si substrate as used for synchrotron optics. The AFM images (1 and 10 μm scans are given) of the MRF processed Si surface ((a) and (c)) show pronounced tool marks and contaminations. After IBS the surface roughness is reduced by a factor of approximately 3–4 ((b) and (d)). From the PSD graph (e) it can be found that surface smoothing operates at all spatial frequencies covered by the AFM measurements ($f = 1 \times 10^{-4}$ nm^{-1}–0.256 nm^{-1}, corresponding to AFM scan sizes of 1 μm and 10 μm, respectively). The processing conditions were Ar^+, $E_{ion} = 500$ eV, $\alpha_{ion} = 45°$, $j_{ion} = 300$ μA cm^{-2}, simultaneous sample rotation.

nents for EUV lithography. For example, EUVL mask blanks require an extreme flatness of 32 nm peak to valley, not only on the front side mask blank but also on the back [21]. Furthermore, thermal expansion of the mask material caused by EUV absorption must be avoided to minimize potential overlay errors. Therefore, near zero thermal expansion materials have to be used as substrate materials. One of the candidate materials is Zerodur®, which is a glasslike SiO_2 ceramic with a completely non-directional, isotropic structure [112]. Due to the well-balanced mixture of glass and crystal phases within the material, the thermal expansion coefficient is nearly zero. The material contains a certain percentage of nano-sized β-quartz crystallites embedded within an amorphous silica phase.

In general, the accuracy of mechanical polishing techniques for this material is not sufficient for achieving the required precision. In order to meet the extreme accuracy demands related to the surface flatness or figure of the specific optical elements, ion beam figuring can be applied as a final correction technique. However, Zerodur® is one of the problem materials mentioned above because ion beam figuring of this material is generally accompanied by increase of the surface roughness (HSFR) even in cases where only a thin surface layer is removed by the ion beam [113, 114]. It is assumed that the roughness evolution in this material is triggered by the different sputter yields of the β-quartz crystallites on the one hand and the amorphous SiO_2 phase on the other.

Therefore, we developed a method in which the deposition of a sacrificial layer, an ion beam planarization step and a final ion beam direct smoothing step have been combined such that the desired final HSFR can be achieved [113, 115]. The overall process is illustrated in figure 11. The starting point is a Zerodur® substrate after it has gone through an IBF procedure (figure 11(a)). Because of the figure correction process the rms surface roughness (HSFR) is increased to $R_q \sim 0.4$ nm, compared to $R_q < 0.2$ nm as measured for the conventionally polished surface before the IBF polishing error correction. In a first step the initially rough substrate is coated with a Si layer by ion beam sputter deposition. Due to the Si coating, the surface roughness is already reduced from ~0.4 nm to an R_q value of <0.2 nm measured for surface areas of 1×1 μm^2 (figure 11(b)). Afterward the surface was smoothed by a planarization step (Ar^+, $E_{ion} = 700$ eV, $\alpha_{ion} = 45°$, standard photoresist as planarizing layer) followed by ion beam direct smoothing. Consequently, the surface roughness decreases to $R_q = (0.142 \pm 0.007)$ nm (figure 11(c)), which is now within the specification as required for HSFR for such optical elements. The given errors correspond to standard deviations obtained from at least ten AFM measurements at different positions on a two-inch substrate. From the PSD graph presented in (figure 11(d)) it is seen that surface smoothing is achieved for all spatial frequencies $f > 1 \times 10^{-4}$ nm^{-1}.

As a result of the smoothing process a thin a-Si layer remains on the Zerodur® substrate but this should be no hindrance to further processing of the substrate, because the following Mo/Si multilayer mirror is usually deposited on the optical substrate using a thin a-Si buffer layer.

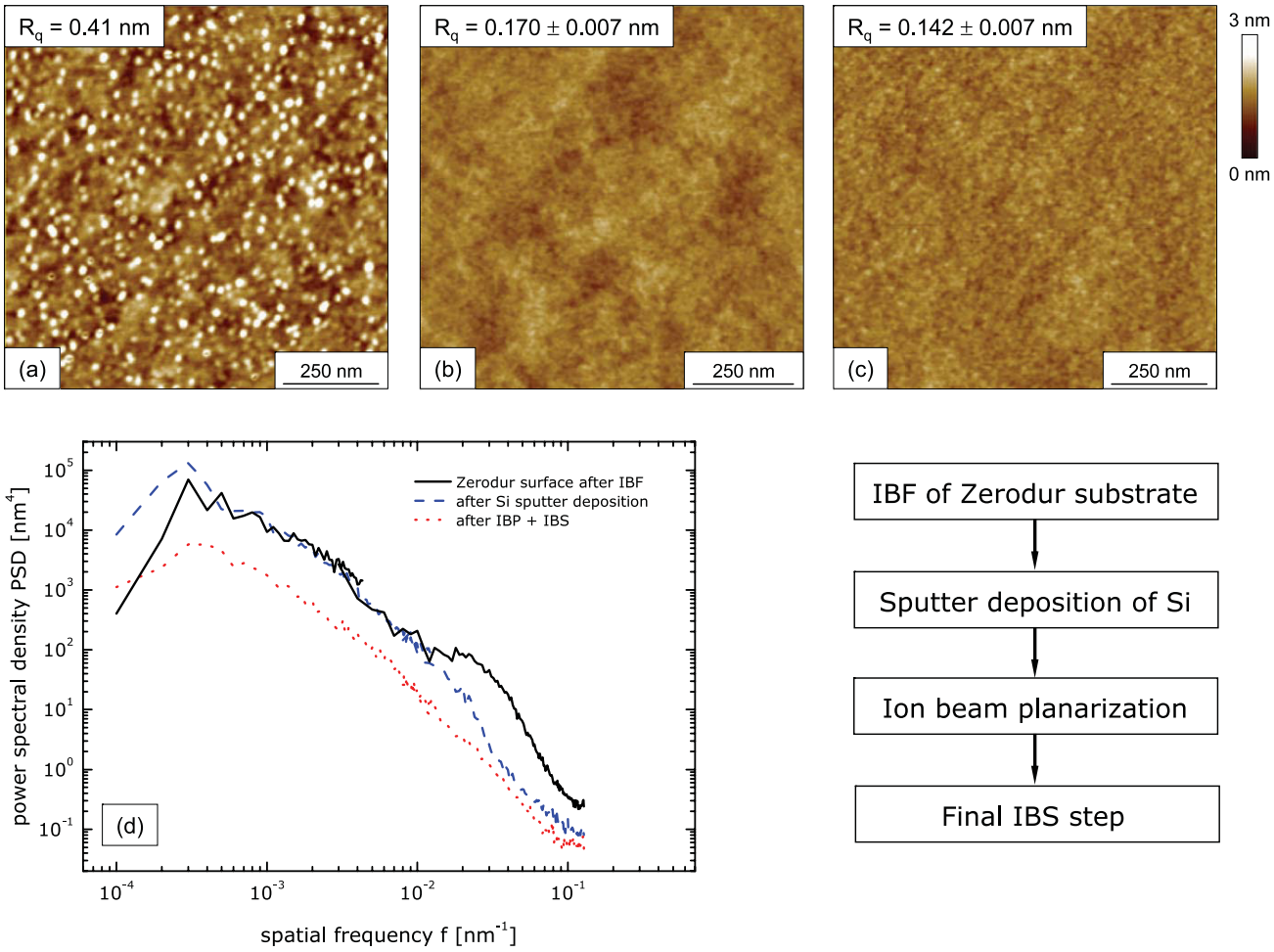

Figure 11. Illustration of the processing sequence of Zerodur® used as substrates for EUVL optical elements. In a first step a shape correction was made by ion beam figuring (IBF). Due to the special composition of Zerodur® this results in an increased surface roughness (a) outside of the specification (HSFR < 0.15 nm rms). In the second step the substrate is coated with a thin a-Si layer by ion beam sputtering, where the surface roughness is reduced to 0.17 nm rms (b). Finally an ion beam planarization and an ion beam direct smoothing step were applied. The final HSFR is now <0.15 nm rms. The error values given correspond to the standard deviations obtained from at least ten measurements on a two-inch substrate. From the PSD graph (d) it is seen that surface smoothing is achieved for all spatial frequencies that are $> f = 1 \times 10^{-4}$ nm^{-1}.

5.3. Smoothing of single-crystal diamond turned metal surfaces

In optical fabrication, single-crystal diamond turning is effectively used to cut metal surfaces to obtain smooth and highly accurate surfaces relevant for different types of mirrors for x-ray and neutron optics or as molds for pressing or injection of optical elements made from glass or polymers. In the EUV lithography, systems with superior optical characteristics are required, for example illumination systems with aspherical surfaces or mirror substrates with more complicated shapes, such as multifaceted fly-eye mirrors [116]. Because these illumination elements are positioned close to the EUV source, increased thermal loads arise as compared to the case for optical projection elements. Therefore, components made of metals for active cooling are preferred. However, typically, single-crystal diamond turned metal surfaces have a surface roughness of 2 nm rms, which reduces their EUV reflectance to only a few per cent, thus hindering their application in such devices. This roughness is mainly caused by the tool marks forming along the tool paths. With the EUVL application, smoothing of those surfaces is inevitably required in order to remove such tool marks. To remove them, in general, wet polishing with abrasives is performed, but this process is very time-consuming. Moreover, wet polishing often generates additional scratches on the surface, which leads to difficulties in polishing metal surfaces to ultrahigh smoothness, especially for copper surfaces.

Therefore, we have expended a great deal of effort in the development and customization of ion beam assisted smoothing techniques for an efficient removal of tool marks from single-crystal diamond turned metal surfaces. The different smoothing steps involved have to be adapted to the material properties as well as surface finishing requirements [117, 118]. In the following, results are presented for single-crystal diamond turned electroless plated NiP coatings. Figure 12(a) shows an AFM image of the initial NiP surface after diamond turning with characteristic

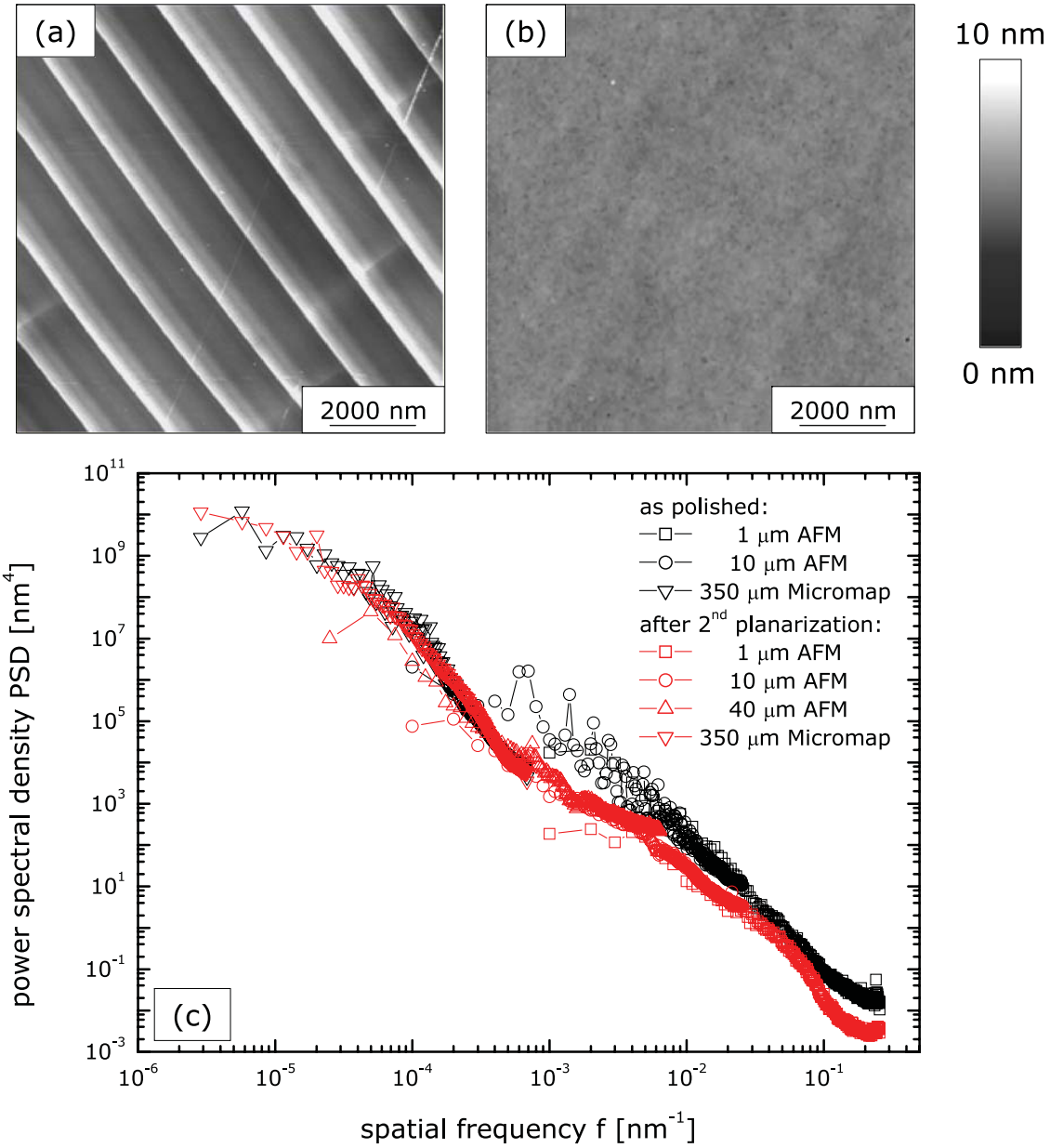

Figure 12. Smoothing of a single-point diamond turned NiP surface by a combination of ion beam planarization and ion beam direct smoothing. Image (a) shows the initial NiP surface with characteristic tool marks of a spatial wavelength of approximately 1.5 μm; the rms surface roughness was 1.73 nm. After two ion beam planarization runs and a final ion beam direct smoothing step the surface roughness has been reduced to 0.31 nm rms. The power spectral densities in (c) indicate that the tool marks and the overall HSFR were significantly reduced. Due to the combination of optical profilometry (Micromap) and AFM over different squared scans (scan sizes are given in the figure) the surfaces were characterized over five orders of magnitude in spatial frequencies.

tool marks of a spatial wavelength of approximately 1.5 μm corresponding to the applied feed rate of the tool as used for the turning process. The rms surface roughness was approximately 1.7 nm. Then the surface was planarized. In this planarization step, the surface was coated with a suitable photoresist layer using either a spin coater or a spray coating system. Typically, the resist layer thicknesses were 50–80 nm. After baking of the photoresist, the surface was etched using Ar^+ ion beams with ion energy of 700 eV, ion current density of 200 μA cm^{-2}, and a planarization angle of 30°. The etching time for the planarization step was adjusted according to the photoresist thickness in order to minimize the overetching into the material. Overall, this planarization procedure was performed twice. Finally, an additional ion beam direct smoothing step was carried out. As a result, nearly all tool marks are removed, as seen in figure 12(b). This is also evident from the PSD analysis shown in figure 12(c) where all surface features with spatial frequencies $f > 10^{-4}$ nm^{-1} are reduced by the ion beam planarization process. The final surface roughness obtained in the given case was 0.31 nm rms. The degree of smoothing achieved is now sufficient to qualify these ion beam processed surfaces for

further applications, such as use as mirror substrates in EUVL systems.

6. Conclusion and outlook

In conclusion, we have tried to span the wide range from exploration of basic mechanisms of ion beam driven surface relaxation to specific applications of ion beam smoothing technology in ultraprecision surface processing. Therefore, we focused on special scenarios in the topography evolution of surfaces under low energy ion beam erosion where relaxation processes dominate over roughening and pattern formation. Under these circumstances, flat surfaces are stable against ion beam induced surface roughening and, additionally, surface smoothing of initially rough surfaces can occur.

Starting with a short compilation of different potential mechanisms responsible for surface smoothing at nanometer and micron length scales, selected relevant relaxation mechanisms were illustrated on the basis of our recent experimental work. Thus examples have been given of smoothing by surface gradient dependent sputtering for III/V semiconductors, ballistic drift motivated smoothing of Si surfaces and the impact of sample rotation for the topography evolution of quartz glass surfaces, and a discussion given. Additionally, it has been shown that by implementing experimental conditions for which surface smoothing dominates, ion beam erosion can be utilized for a well directed reduction of surface roughness of different materials and for the preparation of ultrasmooth surfaces for many other technologically important materials and related applications. In this regard, it is essential to use sophisticated broad beam ion sources with appropriate beam dimensions or suitable process routines to make large area processing feasible.

However, for a practical implementation of this technique, some technological constraints exist, related to the efficiency of smoothing of larger length scale features or the smoothing of some problematic materials like composites or metals. Nevertheless, the physical constraints can be relaxed with the help of further ion beam assisted smoothing techniques, including ion beam planarization or ion beam smoothing of sacrificial layers. Due to the combination of ion beam direct smoothing and ion beam planarization together with a potential use of additional sacrificial layers, smoothing from the atomistic scale up to some tens of microns in spatial wavelength for various materials can be achieved.

In the last few years, a technological basis was developed allowing now for the preparation of ultrasmooth surfaces for a variety of technologically important materials, for example Zerodur® which is used as a substrate for EUVL mask blanks, and different metal surfaces that are important for EUVL or x-ray optics. The techniques developed together with the finishing results obtained so far show that ion beam smoothing technologies are advanced and powerful tools for present and future surface processing and finishing in ultraprecision technology.

Finally, it should be pointed out that further detailed studies of surface smoothing could give more insights into surface relaxation processes, which are also important for understanding the pattern formation processes under ion beam erosion.

Overall, low energy ion beams offer unique and intriguing capabilities for surface topography engineering at nanometer and micron length scales, which qualifies the ion beam as a versatile tool for a wide variety of future applications in nanotechnology.

Therefore, IOM will continue in this field in both basic and technology oriented research and development for further progress in atomic beam related technologies, with a focus on ultraprecision surface smoothing and patterning.

Acknowledgments

Contributions to this work by Dr W Frank, Dr T Hänsel, D Hirsch, I Herold and K Ohndorf are gratefully acknowledged. We are deeply grateful for the fruitful cooperation with Dr S Ritter, Dr J Alkemper and Dr M Schweizer (Schott Glas AG, Germany) and Dr H Takino, Dr N Ohi and Dr K Nomura (Nikon Corporation, Japan). We thank H Neumann, Dr M Tartz, Dr B Faust and F Scholze for very useful discussions concerning broad beam ion sources and technical support with the ion grid systems. The authors would also like to thank Dr M Helgert (Carl Zeiss AG, BS Jena) for providing the masked Si gratings. The financial support of part of the work from Deutsche Forschungsgemeinschaft (FOR 365, FR 1476-2, FOR 845), Ministry of Science and Art of Saxony (4-7541.83-IOM=504), Schott Glas AG and Nikon Corporation is highly appreciated.

References

[1] Carter G 2001 *J. Phys. D: Appl. Phys.* **34** R1
[2] Valbusa U, Boragno C and Buatier de Mongeot F 2002 *J. Phys.: Condens. Matter* **14** 8153
[3] Makeev M A, Cuerno R and Barabási A-L 2002 *Nucl. Instrum. Methods* B **197** 185
[4] Chan W L and Chason E 2007 *J. Appl. Phys.* **101** 121301
[5] Muñoz-García J, Vázquez L, Cuerno R, Sánchez-García J A, Castro M and Gago R 2007 Self-organized surface nanopatterning by ion beam sputtering *Lecture Notes on Nanoscale Science and Technology* ed Z Wang (Heidelberg: Springer) at press arXiv:0706.2625v1
[6] Frost F, Ziberi B, Schindler A and Rauschenbach B 2008 *Appl. Phys.* A **91** 551
[7] Zinner E 1980 *Scanning* **3** 57
[8] Carter G, Gras-Marti A and Nobes M J 1982 *Radiat. Eff.* **62** 119
[9] Wittmaack K 1984 *Vacuum* **34** 119
[10] Wittmaack K 1985 *J. Vac. Sci. Technol.* A **3** 1350
[11] Carter G, Nobes M J and Katardjiev I V 1990 *Surf. Interface Anal.* **15** 447
[12] Karen A, Okuno K, Soeda F and Ishitani A 1991 *J. Vac. Sci. Technol.* A **9** 2247
[13] MacLaren S W, Baker J E, Finnegan N L and Loxton C M 1992 *J. Vac. Sci. Technol.* A **10** 486
[14] Vajo J J, Doty R E and Cirlin E-H 1996 *J. Vac. Sci. Technol.* A **14** 2709

[15] Wittmaack K 1998 *J. Vac. Sci. Technol.* B **16** 2776
[16] Pearton S J 1994 *Int. J. Mod. Phys.* B **8** 1781
[17] Brown N J 1986 *Annu. Rev. Mater. Sci.* **16** 371
[18] Corbett J, McKeown P A, Peggs G N and Whatmore R 2000 *Ann. CIRP* **49** 523
[19] De Chiffre L, Kunzmann H, Peggs G N and Lucca D A 2003 *Ann. CIRP* **52** 561
[20] Moseler M, Gumbsch P, Casiraghi C, Ferrari A C and Robertson J 2005 *Science* **309** 1545
[21] Wu B and Kumar A 2007 *J. Vac. Sci. Technol.* B **25** 1743
[22] Hector S and Mangat P 2001 *J. Vac. Sci. Technol.* B **19** 2612
[23] Gwyn C W, Stulen R, Sweeney D and Attwood D 1998 *J. Vac. Sci. Technol.* B **16** 3142
[24] Smith B W, Venkataraman P, Kurinec S K and Mackay R S 1998 *Proc. SPIE* **3331** 544
[25] Bajt S, Alamceda J, Barbee T, Clift W M, Folta J A, Kaufmann B and Spiller E 2001 *Proc. SPIE* **4506** 65
[26] Kleineberg U, Westerwalbesloh T, Wehmeyer O, Sundermann M, Brechling A, Heinzmann U, Haidl M and Mullender S 2001 *Proc. SPIE* **4506** 113
[27] Chassé T, Neumann H, Ocker B, Scherer M, Frank W, Frost F, Hirsch D, Schindler A, Wagner G, Lorenz M, Otto G, Zeuner M and Rauschenbach B 2003 *Vacuum* **71** 407
[28] Allen L N and Romig H W 1990 *Proc. SPIE* **1333** 22
[29] Schindler A, Hänsel T, Flamm D, Frank W, Böhm G, Frost F, Fechner R, Bigl F and Rauschenbach B 2001 *Proc. SPIE* **4440** 217
[30] Hänsel T, Frost F, Nickel A and Schindler A 2007 *Vak. Forsch. Prax.* **19** 24
[31] Giuliano C 1972 *Appl. Phys. Lett.* **21** 39
[32] Hoffman R A, Lange W J and Choyke W J 1975 *Appl. Opt.* **14** 1803
[33] House II R A, Bettis J R and Guenther A H 1977 *Appl. Opt.* **16** 1486
[34] Spiller E 1989 *Appl. Phys. Lett.* **54** 2293
[35] Puik E J, van der Wiel M J, Verhoeven J and Zeijlemaker H 1990 *Thin Solid Films* **193/194** 782
[36] Kloidt A, Stock H J, Kleineberg U, Döhring T, Pröpper M, Schmiedeskamp B and Heinzmann U 1993 *Thin Solid Films* **228** 154
[37] Schlatmann R, Lu C, Verhoeven J, Puik E J and van der Wiel M J 1994 *Appl. Surf. Sci.* **78** 147
[38] Schlatmann R, Shindler J D and Verhoeven J 1996 *Phys. Rev.* B **54** 10880
[39] Hiruma K, Miyagaki S, Yamaguchi A and Nishiyama I 2007 *J. Vac. Sci. Technol.* B **25** 1554
[40] Beck P A, Ross B F P, Demokritov S O and Hillebrands B 2005 *J. Magn. Magn. Mater.* **290/291** 1108
[41] Mitra P and Hebard A F 2005 *Appl. Phys. Lett.* **86** 063108
[42] Taniguchi N 1974 On the basic concept of nanotechnology *Proc. ICPE (Tokyo)*
[43] Taniguchi N, Kohno T, Maruyama K, Iizuka K, Miyamoto I and Dohi T (ed) 1996 *Nanotechnology: Integrated Processing Systems for Ultra-precision and Ultra-Fine Products* (Oxford: Oxford University Press)
[44] Sigmund P 1969 *Phys. Rev.* **184** 383
[45] Sigmund P 1973 *J. Mater. Sci.* **8** 1545
[46] Tong W M and Williams R S 1994 *Annu. Rev. Phys. Chem.* **45** 401
[47] Herring C 1950 *J. Appl. Phys.* **21** 301
[48] Mullins W W 1957 *J. Appl. Phys.* **28** 333
[49] Mullins W W 1959 *J. Appl. Phys.* **30** 77
[50] Bradley R M and Harper J M E 1988 *J. Vac. Sci. Technol.* A **6** 2390
[51] Carter G and Vishnyakov V 1996 *Phys. Rev.* B **54** 17647
[52] Erlebacher J, Aziz M J, Chason E, Sinclair M B and Floro J A 1999 *Phys. Rev. Lett.* **82** 2330
[53] Erlebacher J, Aziz M J, Chason E, Sinclair M B and Floro J A 2000 *J. Vac. Sci. Technol.* A **18** 115
[54] Erlebacher J, Aziz M J, Chason E, Sinclair M B and Floro J A 2000 *Phys. Rev. Lett.* **84** 5800
[55] Makeev M A and Barabási A L 1997 *Appl. Phys. Lett.* **71** 2800
[56] Carter G 1999 *Phys. Rev.* B **59** 1669
[57] Chason E, Mayer T M, Kellerman B K, McIlroy D T and Howard A J 1994 *Phys. Rev. Lett.* **72** 3040
[58] Umbach C C, Headrick R L and Chang K C 2001 *Phys. Rev. Lett.* **87** 246104
[59] Orchard S E 1962 *Appl. Sci. Res.* **11A** 451
[60] Mayer T M, Chason E and Howard A J 1994 *J. Appl. Phys.* **76** 1633
[61] Mayer T M, Adams D P, Vasile M J and Archuleta K M 2005 *J. Vac. Sci. Technol.* A **23** 1579
[62] Zhou H, Wang Y, Zhou L, Headrick R L, Özcan A S, Wang Y, Özaydin G and Ludwig K F 2007 *Phys. Rev.* B **75** 155416
[63] Vauth S and Mayr S G 2007 *Phys. Rev.* B **75** 224107
[64] Vauth S and Mayr S G 2008 *Phys. Rev.* B **77** 155406
[65] Carter G 1998 *Vacuum* **49** 285
[66] Hirata A, Tokura H and Yoshikawa M 1992 *Thin Solid Films* **212** 43
[67] Holzwarth M, Wissing M, Simeonova D S, Tzanev S, Snowdon K J and Yordanow O I 1995 *Surf. Sci.* **331–333** 1093
[68] Wissing M, Batzill M and Snowdon K J 1997 *Nanotechnology* **8** 40
[69] Kimura K, Fukui A, Nakajima K and Mannami M 1999 *Nucl. Instrum. Methods* B **148** 149
[70] Hansen H, Polop C, Michely T, Friedrich A and Urbasek M 2004 *Phys. Rev. Lett.* **92** 246106
[71] Carter G, Nobes M J and Katardjiev I V 1992 *Phil. Mag.* B **66** 419
[72] Barber D J 1970 *J. Mater. Sci.* **5** 1
[73] Zalar A 1985 *Thin Solid Films* **124** 223
[74] Cirlin E-H, Vajo J J, Doty R E and Hasenberg T C 1991 *J. Vac. Sci. Technol.* A **9** 1395
[75] Bradley R M and Cirlin E-H 1996 *Appl. Phys. Lett.* **68** 3722
[76] Bradley R M 1996 *Phys. Rev.* E **54** 6149
[77] Ziberi B, Cornejo M, Frost F and Rauschenbach B 2009 *J. Phys.: Condens. Matter* **21** 224003
[78] Zeuner M, Meichsner J, Neumann H, Scholze F and Bigl F 1996 *J. Appl. Phys.* **80** 611
[79] Tartz M, Hartmann E, Scholze F and Neumann H 1998 *Rev. Sci. Instrum.* **69** 1147
[80] Barber D J, Frank F C, Moss M, Steeds J W and Tsong I S T 1973 *J. Mater. Sci.* **8** 1030
[81] Malherbe J B 1994 *CRC Crit. Rev. Solid State Mater. Sci.* **19** 55
[82] Facsko S, Dekorsy T, Koerdt C, Trappe C, Kurz H, Vogt A and Hartnagel H L 1999 *Science* **285** 1551
[83] Frost F, Schindler A and Bigl F 2000 *Phys. Rev. Lett.* **85** 4116
[84] Frost F, Ziberi B, Höche T and Rauschenbach B 2004 *Nucl. Instrum. Methods* B **216** 19
[85] Katzschner W, Niggebrügge U, Löffler R and Schröter Janssen H 1986 *Appl. Phys. Lett.* **48** 230
[86] Frost F, Schindler A and Bigl F 1998 *Semicond. Sci. Technol.* **13** 523
[87] Hecht J-D, Frost F, Chassé T, Hirsch D, Neumann H, Schindler A and Bigl F 2001 *Appl. Surf. Sci.* **179** 197
[88] Frost F, Schindler A and Bigl F 1998 *Appl. Phys.* A **66** 663
[89] Frost F, Lippold G, Otte K, Hirsch D, Schindler A and Bigl F 1999 *J. Vac. Sci. Technol.* A **17** 793
[90] Frost F, Schindler A, Hirsch D and Bigl F 1999 *Precision Science and Technology for Perfect Surfaces* ed Y Furukawa, Y Mori and T Kataoka (Tokyo: The Japan Society for Precision Engineering) p 612
[91] Nobes M J, Colligon J S and Carter G 1969 *J. Mater. Sci.* **4** 730

[92] Carter G, Colligon J S and Nobes M J 1971 *J. Mater. Sci.* **6** 115
[93] Carter G, Nobes M J and Whitton J L 1978 *J. Mater. Sci.* **13** 2725
[94] Carter G 1976 *J. Mater. Sci.* **11** 1091
[95] Carter G 1996 *Vacuum* **47** 409
[96] Ziberi B 2006 Ion beam induced pattern formation on Si and Ge surfaces *PhD Thesis* University of Leipzig, Engelsdorfer Verlag 2007
[97] Davidovitch B, Aziz M J and Brenner M P 2007 *Phys. Rev.* B **75** 205420
[98] Drotar J T, Zhao Y-P, Lu T-M and Wang G-C 2000 *Phys. Rev.* B **61** 3012
[99] Frost F, Ziberi B and Rauschenbach B 2009 at press
[100] Eckstein W 1991 *Computer Simulation of Ion–Solid Interactions* (*Springer Series in Material Science* vol 10) (Berlin: Springer)
[101] Facsko S, Bobek T, Stahl A, Kurz H and Dekorsy T 2004 *Phys. Rev.* B **69** 153412
[102] Flamm D, Frost F and Hirsch D 2001 *Appl. Surf. Sci.* **179** 95
[103] Frost F, Voellner J and Flamm D 2009 at press
[104] Toma A, Buatier de Mongeot F, Bruzio R, Firpo G, Bhattacharyya S R, Boragno C and Valbusa U 2005 *Nucl. Instrum. Methods* B **230** 551
[105] Johnson L F, Ingersoll K A and Kahng D 1982 *Appl. Phys. Lett.* **40** 636
[106] Johnson L F and Ingersoll K A 1983 *Appl. Opt.* **22** 1165
[107] Fechner R, Schindler A, Hänsel T and Bigl F 1999 *Precision Science and Technology for Perfect Surfaces* ed Y Furukawa, Y Mori and T Kataoka (Tokyo: The Japan Society for Precision Engineering) p 249
[108] Soufli R, Spiller E, Schmidt M A, Robinson J C, Baker S L, Ratti S, Johnson M A and Gullikson E M 2004 *Proc. SPIE* **5193** 98
[109] Overdiep W S 1986 *Prog. Org. Coat.* **14** 159
[110] Frost F, Fechner R, Flamm D, Ziberi B, Frank W and Schindler A 2004 *Appl. Phys.* A **78** 651
[111] Schindler A, Hänsel T, Nickel A, Thomas H-J, Lammert H and Siewert F 2003 *Proc. SPIE* **5180** 64
[112] http://www.schott.com/lithotec/english/products/Zerodur/Zerodur.html
[113] Frost F, Fechner R, Ziberi B, Flamm D and Schindler A 2004 *Thin Solid Films* **459** 100
[114] Kurashima Y, Uozumi R, Miyamoto I, Ando M and Numata A 2007 *J. Vac. Sci. Technol.* B **25** 2104
[115] Aschke L, Schweizer M, Alkemper J, Schindler A, Frost F, Hänsel T and Fechner R 2004 Substrate for the micro-lithography and process of manufacturing thereof *US Patent Specification* 7,279,252 B2
[116] Hashimoto Y, Takeuchi Y, Kawai T, Sawada K, Takino H and Nomura K 2004 *J. Solid Mater. Mech. Mater. Eng.* C **47** 916
[117] Frost F, Takino H, Fechner R, Schindler A, Ohi N and Nomura K 2006 *Towards the Synthesis of Micro-/Nano-Systems* ed F Kimura and K Horio (Berlin: Springer) p 239
[118] Frost F, Takino H, Fechner R, Schindler A, Ohi N and Nomura K 2007 *Japan. J. Appl. Phys.* **46** 6071